12-2002

Determination of the bremsstrahlung spectra of a clinical linear accelerator using a Simpson iteration technique

Robbie Alhakeem
University of Tennessee

To the Graduate Council:

I am submitting herewith a thesis written by Robbie Alhakeem entitled "Determination of the bremsstrahlung spectra of a clinical linear accelerator using a Simpson iteration technique." I have examined the final electronic copy of this thesis for form and content and recommend that it be accepted in partial fulfillment of the requirements for the degree of Master of Science, with a major in Nuclear Engineering.

Laurence Miller, Major Professor

We have read this thesis and recommend its acceptance:
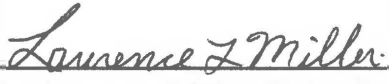
Accepted for the Council:
Carolyn R. Hodges

Vice Provost and Dean of the Graduate School
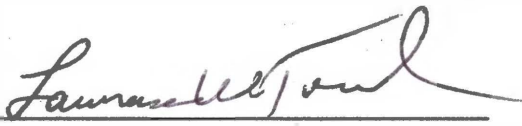
(Original signatures are on file with official student records.)

To The Graduate Council:

I am submitting herewith a thesis written by Robbie Alhakeem entitled "Determination of the Bremsstrahlung Spectra of a Clinical Linear Accelerator using a Simpson Iteration Technique". I have examined the final paper copy of this thesis for form and content and recommend that it be accepted in partial fulfillment of the requirements for the Master's of Science degree in Nuclear Engineering.

Laurence L Miller.

Dr. Laurence Miller, Major Professor

We have read this thesis and
Recommend its acceptance:

Laurence W Townsend

Adrian Oliver, ALO

Accepted for the Council:

Vice Provost and Dean of Graduate Studies

Determination of the Bremsstrahlung Spectra of a

Clinical Linear Accelerator using a Simpson Iteration

Technique

A Thesis
Presented for the
Master of Science
Degree at
The University of Tennessee, Knoxville

Robbie Alhakeem
December 2002

Abstract

X-ray spectral reconstruction from x-ray transmission data was investigated using graphite as an attenuating material which has a monotonic declining mass attenuation coefficient for energies up to 30 MeV, and by employing the numerical method for unfolding spectra. No experimental investigation of energies above 10 MeV using this technique has been performed prior to this research. Previous works utilizing this method have used material such as lead and aluminum which exhibit an increase in attenuation coefficients in the 8 to 10 MeV range and beyond. This increased attenuation leads the Simpson technique to produce a number of non-unique fractional fluencies representing dual energies. Photon energy spectra for 6 MV and 18 MV beams produced by Varian 6100 and Varian 2100C linear accelerators were determined to validate the consistency of the measured data and the modeling method. The resulting Simpson unfolded spectra were compared to the published 6 MV Mohan spectrum and an interpolated 18MV spectrum. Both spectra are Monte Carlo based and used in the ADAC Laboratories three dimensional Pinnacle treatment planning system (3DPRTP). Modal energies for the Simpson technique were determined and compared to the modal energies for the Mohan spectrum and the interpolated 18 MV spectrum. Our method's modal energies for the 6MV beams were similar to the Mohan 6MV spectrum. The modal energies for this work are 0.73 MeV for 2100-6 MV beam and 0.84 MeV

for the 6100. For the 2100-18 MV beam, the modal energy for the determined Simpson spectrum was approximately 4.2 MeV. The Pinnacle (ADAC 3DPRTP) interpolated 18 MV spectral model yield a modal energy of 1.0 MeV. All of the above spectra were also compared to a Huang modified Jones-fit Laplace transform generated energy fluence spectra. The Laplace technique produced modal energies of 1 MeV for the 2100-6 MV beam and .7 MeV for the 6100 photon beams. The 2100-18 MV modal energy for the Laplace technique was 2.5 MeV. The relatively large differences in the modal energies for the 18 MV spectra lead the author to compare the results with a fourth spectral model generated by Francois and Catala through a technique of direct resolution of a matrix system of transmission data. The Francois – Catala technique yields a number of modal energies for 15MV to 20 MV beam spectra ranging from 2.76 to 3.58 MeV. These modal energies agree with the Simpson model as opposed to the interpolated 18 MV model. The HVL data also suggests that the modal energy of the beam is substantially larger than 1 MeV. The disagreement of all the above models leads the author to conclude that further work and unification of methodology is needed to verify true photon energy spectra.

Table of Contents

List of Tables

List of Figures

Chapter 1

Introduction

1.1 Rationale for Determining the Energy Spectrum

Chemical and biologic changes in tissue exposed to ionizing radiation depend more on the energy absorbed than on the amount of ionization the radiation produces in air. Dose from ionizing radiation is defined as the amount of energy absorbed from the imparted energy per unit mass to a small volume of the irradiated medium. The modern radiotherapy linear accelerator (Linac) produces several monochromatic electron beams and photon beams. This allows for a range of dose distributions to match the goals of treatment planning. Photon beams in a Linac are produced via bremsstrahlung interactions of the monochromatic electrons with a tungsten target in the treatment head. These interactions produce a spectrum of photon energies ranging from zero up to the energy of the incident electron beam, and the shape of the energy spectrum directly affects dose deposition in a medium. The spectral distribution of photons for each Linac is unique for a specific configuration. The measured photon energy spectrum is dependent on the target, flattening filter, ionization chamber, and bending magnet. Because of slight variations in manufacturer tolerance, the x-ray spectrum from two accelerators of the same design operating at the same monochromatic electron energy may be different.

1.2 Problems and Methods of Determining Clinical Photon Spectra

A reliable method of determining the energy spectrum is desirable especially for three-dimensional (3-D) treatment planning. Direct measurement of the high energy photon beam spectrum using scintillation detectors such as NaI (Tl) or Ge (Li) is difficult due to the high dose rates produced, and the detector low collection efficiency due to the large range in energy of the photons produced. However, measurements have been attempted, using both direct and indirect techniques. One method places a scatterer at an angle with the primary axis and perpendicular to NaI (Tl) detector (Levy et al 1975, Brownridge et al 1984, Landry and Anderson 1991). Monte Carlo calculations have been used also to theoretically determine the energy spectra (Mohan et al 1985, Kan et al 1987, Chaney et al 1994). Monte Carlo techniques are considered the gold standard for simulating the production of the bremsstrahlung spectrum, and the interaction of the photon beam with the beam shaping components in the accelerator head. Computer Programs such as the EGS4, BEAM, and ITS (ETRAN) simulate electromagnetic cascades in various geometries. They have the ability to realistically model radiation transport of photons and electrons in a variety of elements, compounds or mixtures. However, the results of these programs are highly dependent on the level of detailed description of the accelerator head design. A common approach is to separate the model into a series of individual component modules (CMs), each of which operates independently of the other component modules and occupies a slab at right angles with the beam axis. The computer computational times are typically in the range of several hours, today, as compared to 600 hours on a VAX 11/780 (D.W.O Rogers et al 1994).

2

The time constraint and the specific knowledge of geometrical and material makeup of the head design makes this method rather complicated for routine clinical applications.

Determination of the photon spectrum from measured beam parameters has been studied by several investigators. One approach (Bloch and Mcdonough 1997) is to fit calculated data represented as a percent of the point of maximum dose (PDD) from a monoenergetic beam to a measured PDD from a clinical beam. This data is combined with an electron disequilibrium factor in the buildup region to produce a meaningful spectrum. Measured attenuation data has been used to model the photon spectrum from the keV range to the MeV range. Figure 1 illustrates the mass attenuation coefficient of various elements versus energy. Note that for photon energies from the keV up to the low MeV range the photoelectric effect is dominant. The steep decline in attenuation coefficient versus energy for most materials is beneficial in producing a unique signature for an energy spectrum. In the Compton region, common attenuating material such as lead and aluminum experience an increase in the mass attenuation coefficient starting at the 8 to 10 MeV regions and above. Other attenuating material such as water and carbon exhibit a monoenergetic decline of mass attenuation coefficient to well over the 25 MeV range. The rate of decline with energy plays an important role in the ability to use the material for spectral analysis.

Laplace transforms have been used to unfold photon spectra in the photoelectric and Compton regions (Huang et al 1980, Archer et al, 1982). In this method, the x-ray attenuation curve is fitted to an analytical function containing several parameters. If the model is appropriately chosen, its inverse Laplace transform will generate a unique solution of the original spectrum. This method was applied by Silberstein (Huang et al
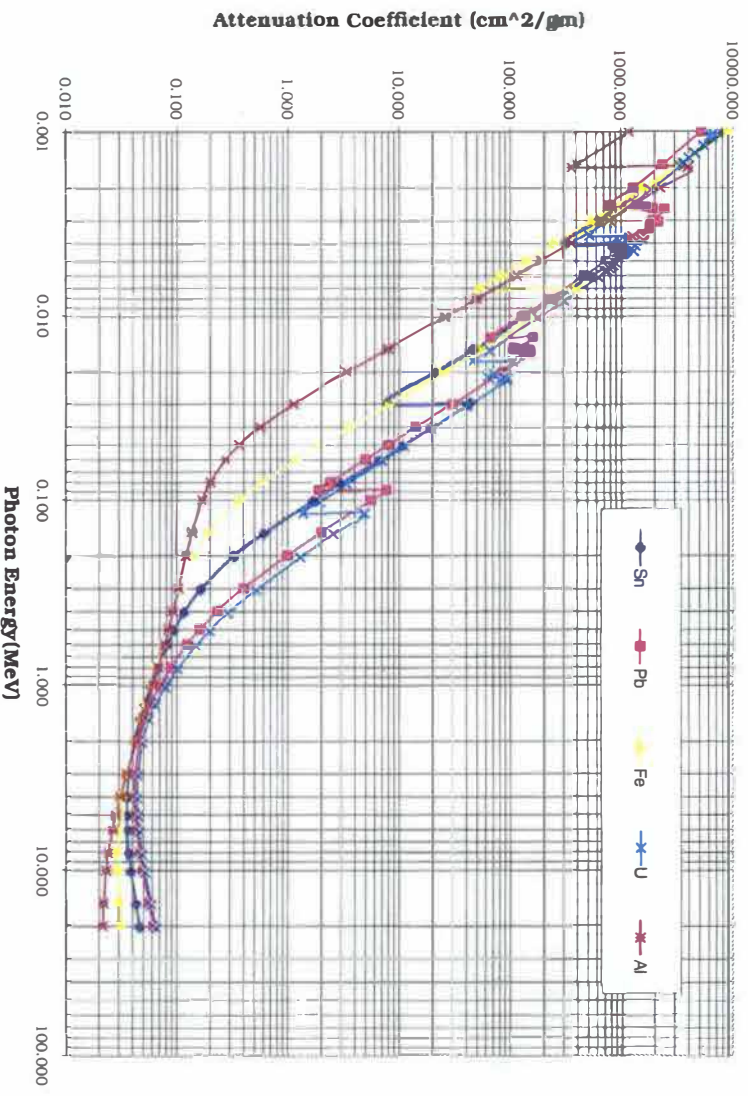
Figure 1. Mass Attenuation Coefficient versus Photon Energy for various elements. (Johns and Cunningham. "The Physics of Radiology", 3rd edition 1969)

investigated in this work. The pair production spectra were not investigated in this work. The pair production spectra were not method spectrum for a 4MV-photon beam. The pair production spectra were not and others. Figure 2 displays a based on Jones method spectrum and a based on Huang method spectrum for a 4MV-photon beam. The pair 1980) and later improved by Jones (Huang et al 1980), Huang et al (Huang et al 1980)

1.3 Work Objectives

In this work an iteration technique that uses the Simpson numerical integration quadrature is developed. This method had been evaluated (Huang et al 1982, Pirametti et

4
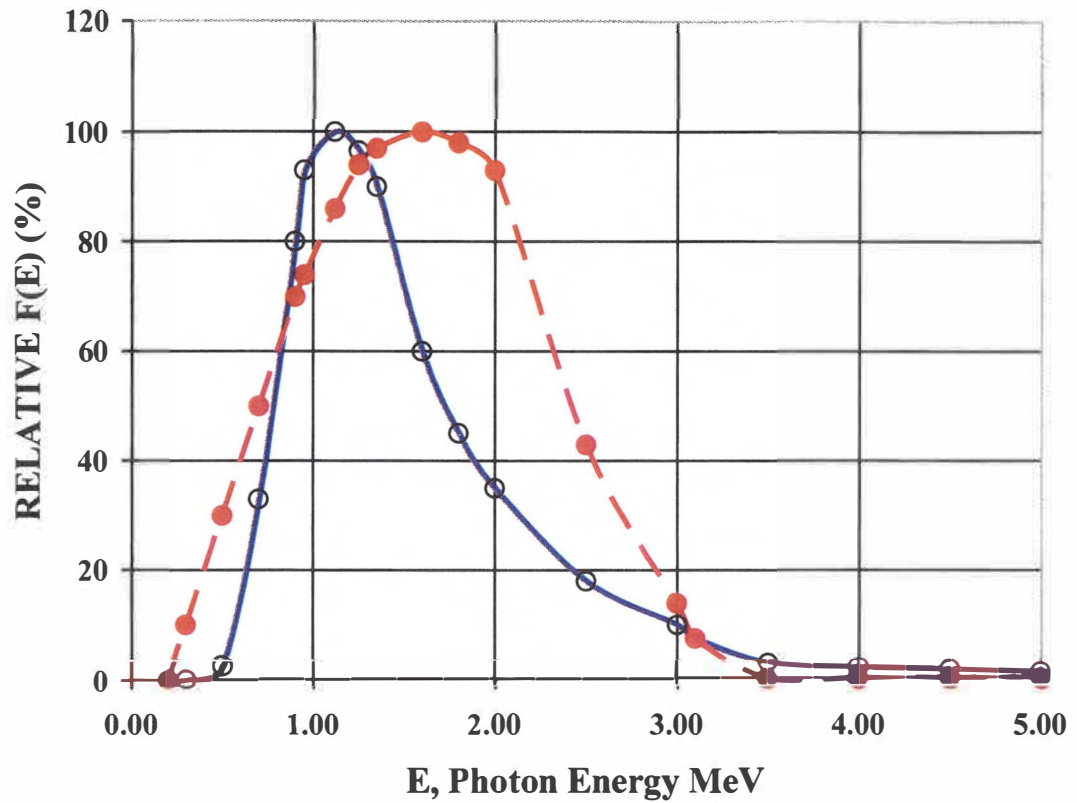
Figure 2. Relative fractional photon fluence F(E) in percent per MeV as a function of photon energy E for a Varian Clinac-4 determined by Huang et al second order polynomial Laplace model(solid curve) vs. a Jones model(dashed curve). (Huang, Kase, and Bjangard: Spectral characterization 1982.)

al 1989), but no experimental investigation of energies above 10 MeV has been performed to date. This is due to the use of material such as lead and aluminum with a limited useful attenuating range vs. energy. The limitation is due to the fact that the attenuation coefficient of both these materials begin to increase above 10MeV, and this produces a non-unique representation of the beam energies as discussed in the Methods and Materials section. The attenuation material chosen for this work is graphite since it does not suffer from such a limitation and energy spectra for a Varian 6100 and 2100C beams were developed from a Simpson spectral unfolding algorithm. The Varian 2100C is a dual energy photon unit with a 6 MV photon beam (2100-6 MV) and an 18 MV photon beam (2100-18 MV). The spectra obtained were compared to spectra used in a Pinnacle three dimensional treatment planning (P3DRTP)system currently used at the Thompson Cancer Survival Center (TCSC). The P3DRTP system is a product of ADAC. ADAC is a manufacturer of Radiation Therapy and Nuclear Medicine equipment located in Milpitas, California. The P3DRTP spectrum is initially assumed to represent a particular machine and then refined by each radiotherapy department through comparing computed and measured open field depth dose curves and by adjusting the spectrum until the shape of the two curves matches. All of the above spectra were also compared to the Huang Laplace transform generated spectrum described in the previous section.

Chapter 2

Theory

2.1 The Bragg-Gray Cavity Theory

The Bragg-Gray cavity theory may be used to calculate the dose directly from ion chamber measurements in a medium. According to the Bragg-Gray theory (Kahn,1994), ionization produced in a gas filled cavity through inelastic collisions of entering primary (produced by photons) and secondary electrons (produced by primary and subsequent generations of electrons), is directly proportional to the energy absorbed in the surrounding medium. The following assumptions are made: the electrons undergoing these collisions are stopped in the chamber, and the chamber must be small enough not to cause a disruption in the distribution of electrons that would exist in the medium without the cavity. Equation 1 describes the conversion of ionization in the gas filled $\frac{\bar{S}}{\rho}$ absorbed dose in the medium by application of the Bragg-Gray principle (Kahn, 1994).

$$D_{med} = J_g * \frac{\overline{W}}{e} * \left(\frac{\bar{S}}{\rho}\right)_g^{medium} \tag{1}$$

D_{med} = the absorbed dose in the medium (in the absence of the cavity)

J_g = the ionization charge of one sign produced per unit mass of the cavity gas

$\left(\frac{\bar{S}}{\rho}\right)_g^{medium}$ = a weighted mean ratio of the mass stopping power of the medium

to that of the cavity gas for the electrons crossing the cavity.

7

$\dfrac{\overline{W}}{e}$ = 33.97 J/C. Average energy required per unit charge of ionization produced in air.

The product of $J_g * \dfrac{\overline{W}}{e}$ is the energy absorbed per unit mass of the cavity gas. The stopping power is defined as the energy loss by electrons per unit path length in a material (Kahn, 1994). The first assumption in the Bragg-Gray theory is inconsistent with the second when using a practical chamber since the chamber has to be large enough to exceed the range of the secondary electrons so that they would not deposit some of their energy in the medium, and small enough not to perturb the distribution of electrons that would exist when the chamber is not present. Hence, Equation 1 is further modified to include the Spencer – Attix theory (Kahn, 1994), or restriction.

2.2 The Spencer-Attix Theory

In this theory (Kahn, 1994) the secondary electrons are divided into two groups that are separated by a cutoff energy Δ that corresponds to the energy of an electron that can just cross the cavity (10 – 20 keV). Below that energy, an electron is considered "Slow" and is assumed to deposit all its energy at the point of its original generation. Hence, the stopping power is redefined as the restricted mass collision power with Δ as the cutoff energy. Equation 2 is based on the Spencer-Attix theory (Kahn, 1994)

$$D_{med} = J_g * \frac{\overline{W}}{e} * \left(\overline{\frac{L}{\rho}} \right)_g^{medium} \qquad (2)$$

8

$$\left(\frac{\overline{L}}{\rho}\right)_{g}^{medium}$$ = Restricted mean mass collision stopping power, averaged over the

electron slowing down spectrum in the wall material.

Practical ionization chambers perturb the photon and electron fluence in various ways. Therefore Equation 2 is further modified to Equation 3 to account for these effects:

$$D_{med} = M * N_{gas} * \left(\frac{\overline{L}}{\rho}\right)_{g}^{medium} * P_{ion} * P_{repl} * P_{wall} \qquad (3)$$

M   = Charge collected
N_{gas} = Dose to the gas per unit charge or electrometer reading.
P_{ion} = Factor that corrects for ionization recombination losses that
    occur at the time of beam calibration. It is the inverse of the collection
    efficiency and has a value of unity or above.
P_{repl} = Replacement correction which depends upon the type and energy
    of the radiation, it is the ratio of photon energy fluence at the
    center of the cavity when the cavity is filled with medium to that when
    the cavity is filled with air.
P_{wall} = Correction factor that accounts for the difference between the
    composition of the chamber wall and the phantom as it pertains
    to photon beam interactions in the users beam.

2.3 Improvement of Dosimetric Accuracy:

Most dosimetry protocols for verification of dose in comparison to Linac output (TG21 1984, IPSM 1990, IAEA 1987) utilize a tissue phantom ratio (TPR) at depths of 10cm and 20 cm to estimate the restricted mass collision stopping power (TG21 1984). Figure 3 illustrates the TPR method of measurement where ionization chamber readings are taken at two depths while the distance between the source and the ionization chamber remains constant.
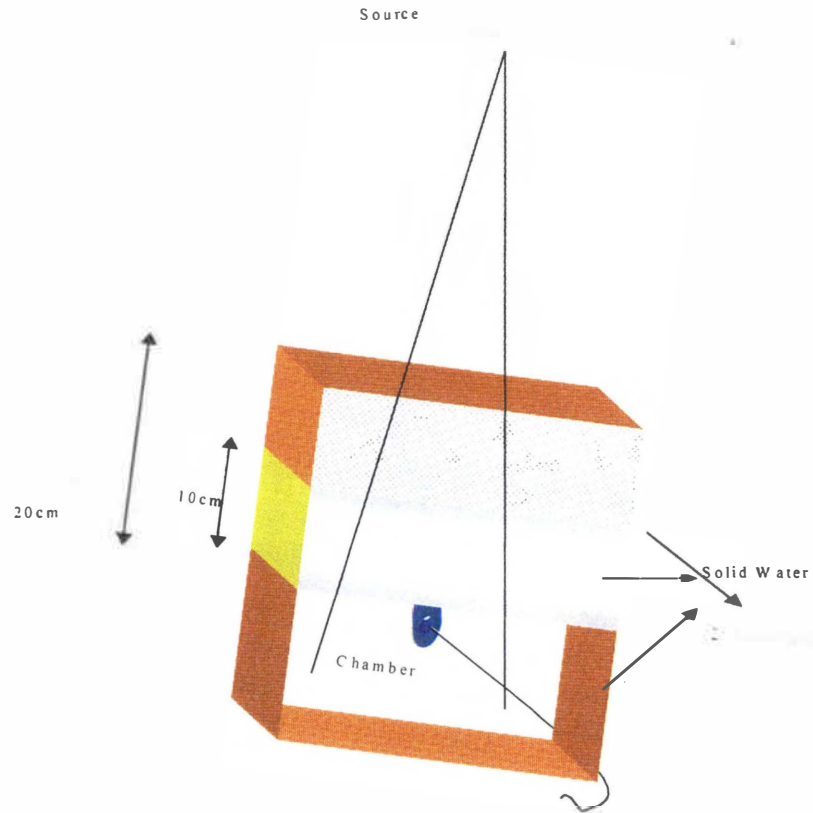
Figure 3. Tissue Phantom Ratio (TPR) method of measurement where ionization chamber readings are taken at two depths while the distance between the source and the ionization chamber remains constant.

The ratio is then correlated with the solid water curve to find the nominal accelerating potential (NAP) and the stopping power, as in Figure 4. (Solid water is a material of equivalent electron density to water. Electron density is the predominant factor in the photon interaction with matter.) The Nominal Accelerating Potential is an agreed upon representation of the average photon beam obtained from a TPR (10 cm depth, and 20 cm depth) versus restricted mass collision stopping power .
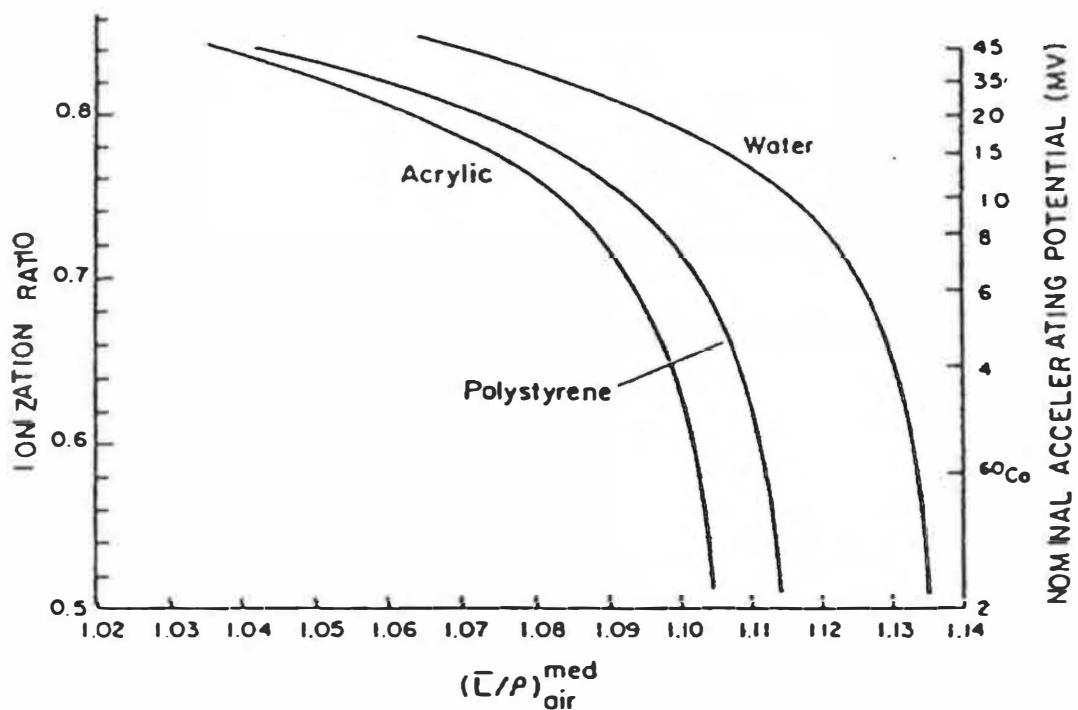
Figure 4. Ratio of mean restricted stopping power for several phantom materials to air as function of the ionization ratio and the nominal accelerating potential. (Taken from TG21, 1984)

In Figure 4 the restricted mass collision stopping power corresponds to a general representation of photon spectra where all beams of the same Nominal accelerating energy are considered equal. Of course this is not the case, since the monochromatic energy of the electrons leaving the exit window of the accelerator structure defines the manufacturer-designated energy of the photon beam, which is transformed into a polyenergetic spectrum. Therefore, dosimetric accuracy would be enhanced if the restricted mass collision stopping power were calculated as a weighted sum of the values of monoenergetic beams (Andreo and Nahum 1985).

Chapter 3

Methods and Materials

3.1 The Simpson Iteration Technique

The basic transmission function for the photon beam is $T(x) = \dfrac{I(x)}{I(0)}$ where I (x) describes the intensity or signal of the beam after an absorber of thickness x. I (0) is the intensity of the beam without an absorber. Equation 4 describes the transmission function of a polyenergetic beam

$$T(x) = \int_{0}^{E_{max}} e^{\mu(E)x} \; F(E) \, dE \qquad (4)$$

Where μ (E) denotes the linear attenuation coefficient at energy E and F (E) is the photon spectrum. According to Huang et al and Pirametti et al, the above equation can be linearly approximated using the Simpson rule to obtain the following:

$$T(x_i) = \frac{\Delta E}{3} * (F_1 \, e^{-\mu_1 x_i} + 4F_2 \, e^{-\mu_2 x_i} + 2F_3 \, e^{-\mu_3 x_i} + 4F_4 \, e^{-\mu_4 x_i} + \cdots + 2F_{(n-2)} \, e^{-\mu_{(n-2)} x_i} + 4F_{(n-1)} \, e^{-\mu_{(n-1)} x_i} + F_n \, e^{-\mu_n x_i}) \qquad (5)$$

In Equation 5, n is the total number of energy groups; and is specified to be odd since the Simpson rule requires an odd number of intervals. $\Delta E = \dfrac{(E_n - E_1)}{(n-1)}$ is the final maximum energy minus the initial energy divided by the number of intervals represented by n-1.

$F(j) = F_1, F_2, F_3, F_4 \dots F_n$ are the fractional values of the spectrum in each energy range, and $\mu(j)$ are the attenuation coefficients for photons of energies Ej. Equation 5 may be written as

$$T(x_i) = \frac{\Delta E}{3} \sum_{j=1}^{n} A_{ij} F_j \qquad (6)$$

Here $A_{ij} = \alpha \, e^{-\mu_i x_i}$ and $\alpha = \begin{cases} 1 & \text{for } j = 1 \text{ and } n \\ 4 & \text{for } j = 2,4,(n-1) \\ 2 & \text{for } j = 3,5,(n-2) \end{cases}$ (7)

One method for solving this equation is a nonlinear least square iteration method (NLSIM). The NLSIM approach assumes a starting spectrum G_j^k, where k denotes the consecutive number of iterations. Thus k = 0 refers to the initial assumed set of fractions F_j which make up G_j^k.

Based on the expected physical shape of a photon spectrum, F_1 through F_n are assumed to rise from F_1 towards a maximum fractional photon fluence and then decrease towards F_n. This maximum fractional photon fluence designates the modal or the most frequently occurring energy in the beam. The transmission factor (C_i^k) is calculated using Equation 5 and compared to T (x_i) using the statistic Chi square (χ^2) (Huang et al 1984).

$$\chi^2 = \sum_{i=1}^{n} \left(\frac{C_i^k - T(x_i)}{\gamma_i T(x_i)} \right)^2 \qquad (8)$$

where $\gamma_i\, T(x_i)$ is the estimated uncertainty and it is equal to one fractional standard deviation of the measured transmission value T (x_i).

$$\gamma_i = \begin{cases} 0.0015 & \text{for} \quad T \geq .05 \\ 0.0050 & \text{for} \quad T < .05 \end{cases}$$

In our own modified Simpson iteration the following procedure is employed:

1. Select a number of equal energy intervals for carbon associated with their respective attenuation coefficients.

2. Begin with an initial spectrum designated as spectrum G_0 which translates to an initial set of fractional photon fluencies. (F_1, F_2, F_3, ... ,Fn) corresponding to the chosen energies.

3. Calculate $F_1' = F_1 \left(\dfrac{T(x_i)}{C_i^k} \right)$ where T (x_i) is a transmission factor for a chosen length and C_i^k is the Simpson iteration calculated transmission factor.

4. Replace G_0 with G_1 which is comprised of ($F1'$, F_1, F_2, F_3 ... Fn).

5. Calculate the transmission factor C_i^k.

6. Calculate $\chi^2 = \sum\limits_{i=1}^{n} \left(\dfrac{C_i^k - T(x_i)}{\gamma_i T(x_i)} \right)^2$

7. If $\chi^{2'} >$ or $=$ to χ^2 undo step 3 and go to step 9.

8. If $\chi^{2'} < \chi^2$, set $\chi^2 = \chi^{2'}$ then go to step 9.

9. Set $j = j + 1$ Repeat 2 through 8 unless if j is $>$ n where n is the total number of fractional photon fluencies. The above part of the iteration is repeated until X^2 is minimized.

No values of $F(E)$ were allowed to be less or equal to zero (Huang et al 1994) in order to obtain a meaningful spectrum with all the factors in Equation 5 larger than zero.

The initial spectrum designated as spectrum G_0 is set to increase towards the modal energy and then decrease. The modal energy or the most frequently occurring energy was designated as the average effective energy which corresponds to a half value layer (HVL) of the transmission data. The HVL is the attenuator thickness in the path of the beam where the signal detected at the collecting chamber is half the original signal. The effective energy is the energy of photons in a monoenergetic beam that is attenuated at the same rate as the heterogeneous photon beam in question. Since the attenuation coefficient curve for a given material is characterized by the slope or linear attenuation coefficient (μ), the effective energy is determined by finding the energy of the monoenergetic photons which have the same (μ) as the given beam. In a heterogeneous beam the 2nd HVL is greater than the first and so on. This is due to the filtering out of the lower energy photons thus resulting in a hardened beam with higher average energy of photons. Each consecutive HVL corresponds to a larger effective energy. In this work we define the modal energy as the average of the effective energies for the 1st, 2nd, and 3rd HVL's.

3.2 The Huang modified Jones Fit Laplace Transform for Resolving Energy Spectra

In this method, an x-ray attenuation data are fitted to an analytical function containing several parameters. If the model is appropriately chosen, its inverse Laplace transform will generate a unique solution that resembles the original spectrum. The modified Jones method developed by Huang et al fits the experimental transmission data $T(x)$ data to the exponential function in Equation 9.

$$T(x) = e^{(-ax + bx^2)} \tag{9}$$

a and b are positive, the inverse Laplace transform of Equation 9 yields Equation 10, a function assumed to fit the spectrum (P.H. Huang et al 1983)

$$f(\mu) = \left(\frac{1}{2\sqrt{\pi b}} \right) e^{\left[\frac{-(\mu - a)^2}{4b} \right]} \tag{10}$$

where:

$f(\mu)$ = Fraction of the total signal produced by photons with attenuation coefficient μ per interval μ in the un-attenuated beam.

$f(\mu)$ is related to $F(E)$ which is the fraction of signal produced by photons of energy E in the range dE through Equation 11

$$F(E) = -f(\mu) \frac{d\mu}{dE} \tag{11}$$

3.3 The Pinnacle 3DPRTP Energy Spectrum Model

The Pinnacle 3DPRTP system contains a number of initial spectra models, which are fine tuned through comparison with the appropriate PDD data .The PDD data can be measured in a Source to Surface Distance geometry (SSD) with the source being 100 cm from the surface of a water phantom (Khan , F.M. 1994). The dose is determined using an ionization chamber that is connected to an electrometer. The maximum dose occurs at the depth of maximum buildup. The equations for determining the electron contamination in relation to depth, off axis distance, and field size effect are displayed in Figure 5.
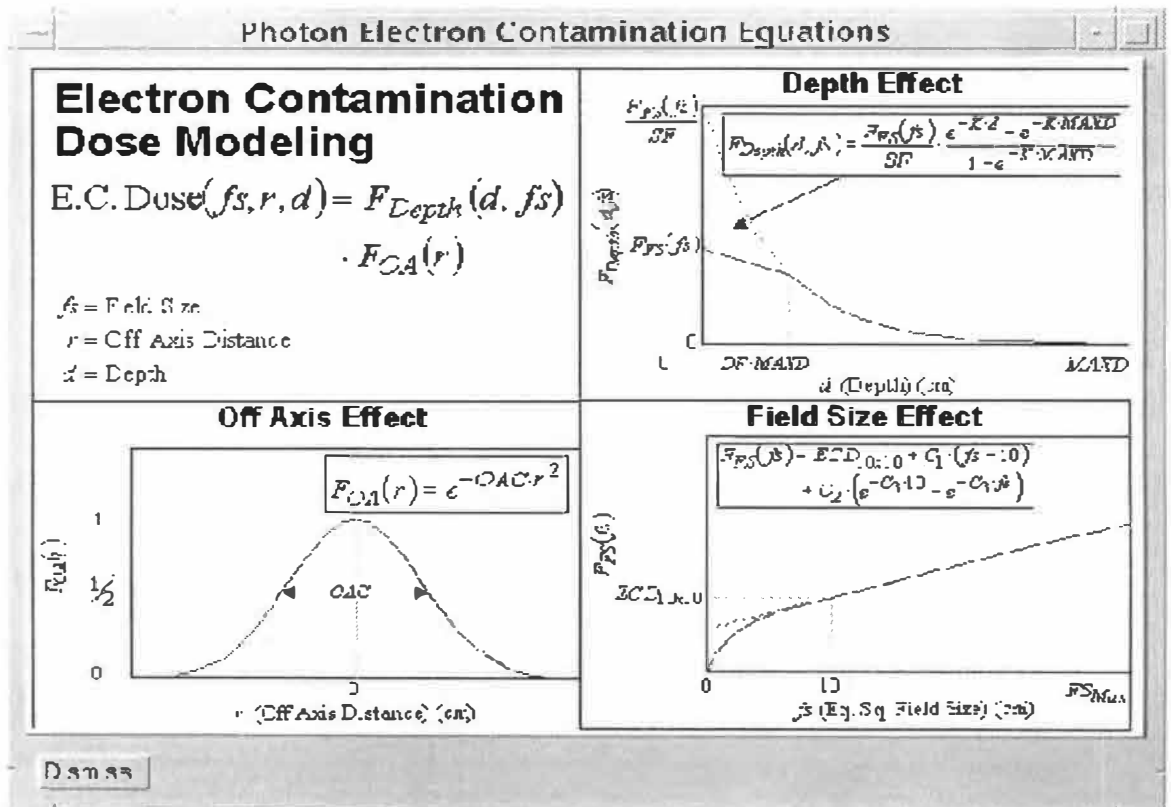
Figure 5. Electron contamination in relation to depth off axis distance and the field size effect.

The spectrum is adjusted until the shape of the two curves matches well. Figure 6 is the Profile Statistics window where the matching of the PDD's is performed. The spectrum in Figure 7 is a Mohan 6MeV photon spectrum (Mohan, R. and C. Chui. 1985) obtained through a Monte Carlo modeling and used as an initial spectrum in Pinnacle. It is first adjusted for the 10x10 cm^2 field size until there is a reasonably good match and then repeated for all the other field sizes. A fine tuning sequence automatically adjusts the relative photons per energy to achieve the final spectrum.
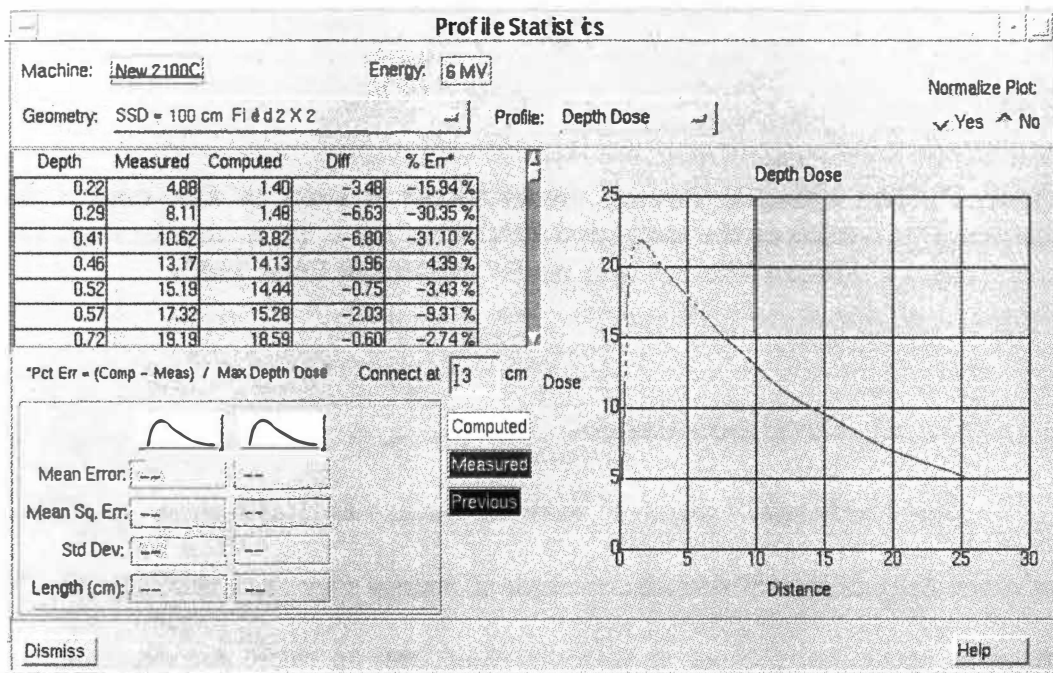
Figure 6. ADAC Laboratories Pinnacle screen for measured versus calculated PDD's. The measured PDD's are adjusted as a direct result of fine tuning the spectrum.
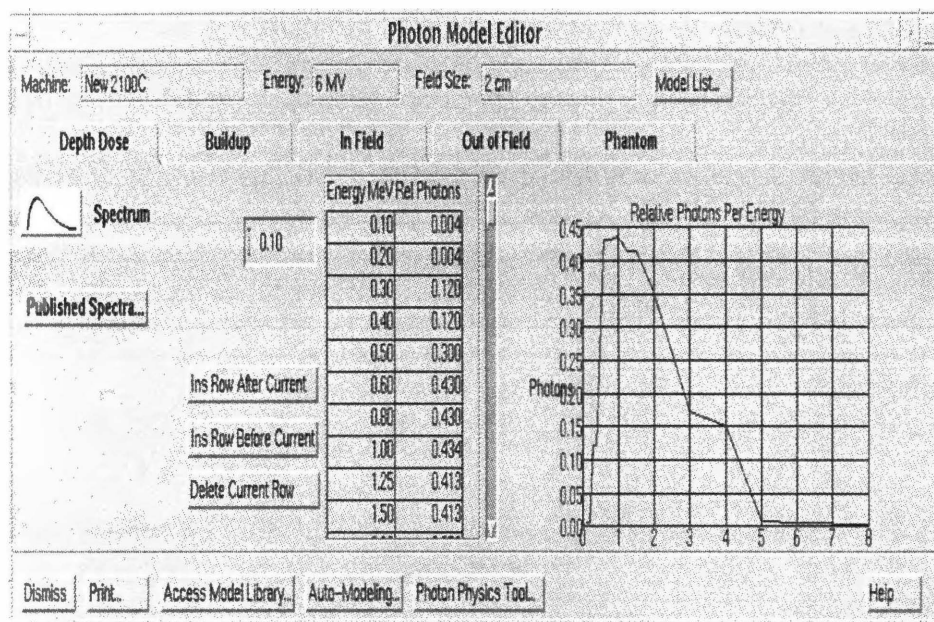
Figure 7. The Pinnacle Photon model editor is used to fine tune a published spectrum to represent the measured PDD data for a linear accelerator. The above spectrum is a Mohan Monte Carlo model (Mohan & Chui, 1985)

3.4 Choice Of Attenuation Material

This technique requires material with an attenuation coefficient that monotonically decreases with the increase in energy over the desired range. The LSIM diverges above energies of 4 MeV for lead and 11 MeV for aluminum since the attenuation coefficient of these materials, μ (E), levels off and begins to increase. This results in most unfolding algorithms yielding a non-unique solution. Our unfolding technique relies on attenuation coefficients as unique value for all energies. For example in the case of an 18 MeV photon beam being attenuated through a medium, both lead and aluminum have attenuation coefficients μ (E) which correspond to two different

energies as seen in Figure 8, where μ (E) would correspond to two energy values E_3 and E_5.

Carbon is more suitable than lead and aluminum for the 12 MeV and above photon beam range since its linear attenuation coefficient has been experimentally verified to decrease monotonically from 0 to 30 MeV. Table 1 and Figure 9 display the mass attenuation coefficients for carbon at various energies.

Mass Attenuation Coefficients
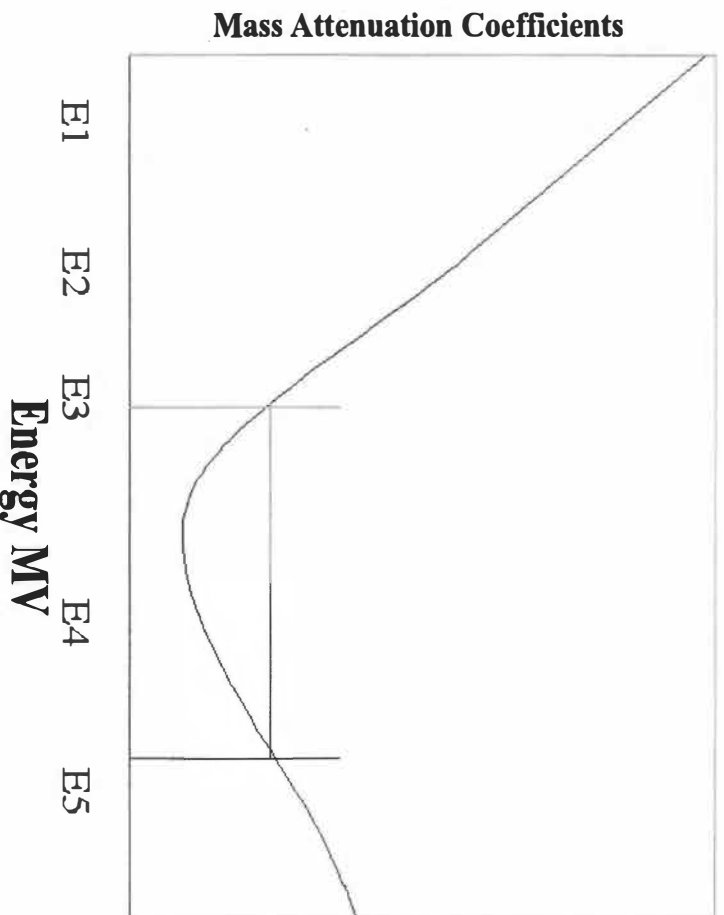
Energy MV

Figure 8. A plot of linear mass attenuation coefficient versus energy demonstrating the non uniqueness of a solution produced by a material which does not posses a monotonically declining attenuation coefficient with increasing energy in the range of interest.

Table 1. Mass attenuation coefficient (μ/ρ) vs. Energy for Carbon (ρ = 2.2 gm/cm³ Taken from The Physics of Radiation therapy, Faiz M Kahn)

Energy MeV	μ/ρ (cm²/g)	Energy MeV	μ/ρ (cm²/g)	Energy MeV	μ/ρ (cm²/g)
0.01	2.1600	3.20	0.0346	6.40	0.0241
0.10	0.1490	3.40	0.0341	6.50	0.0240
0.20	0.1220	3.50	0.0336	6.60	0.0238
0.30	0.1060	3.60	0.0331	6.70	0.0237
0.40	0.0953	3.70	0.0325	6.80	0.0236
0.50	0.0870	3.80	0.0320	6.90	0.0234
0.60	0.0805	3.90	0.0315	7.00	0.0232
0.70	0.0756	4.00	0.0305	7.10	0.0230
0.80	0.0707	4.10	0.0302	7.20	0.0228
0.90	0.0671	4.20	0.0298	7.30	0.0227
1.00	0.0635	4.30	0.0295	7.50	0.0224
1.10	0.0611	4.40	0.0291	7.80	0.0221
1.20	0.0588	4.50	0.0288	7.90	0.0219
1.30	0.0564	4.60	0.0285	8.00	0.0216
1.40	0.0541	4.70	0.0281	10.00	0.0196
1.60	0.0502	4.80	0.0278	11.00	0.0193
1.70	0.0487	4.90	0.0274	12.00	0.0191
1.80	0.0473	5.00	0.0271	13.00	0.0188
1.90	0.0458	5.10	0.0269	14.00	0.0186
2.00	0.0443	5.20	0.0266	15.00	0.0170
2.10	0.0434	5.30	0.0264	16.00	0.0169
2.20	0.0426	5.40	0.0261	17.00	0.0168
2.30	0.0417	5.60	0.0257	18.00	0.0166
2.40	0.0408	5.70	0.0254	19.00	0.0165
2.50	0.0400	5.80	0.0252	20.00	0.0158
2.60	0.0391	5.90	0.0249	21.00	0.0157
2.70	0.0382	6.00	0.0247	21.00	0.0156
2.80	0.0373	6.10	0.0245	22.00	0.0155
2.90	0.0365	6.20	0.0244	24.00	0.0153
3.00	0.0356	6.30	0.0243	25.00	0.0151
3.10	0.0351	6.30	0.0243	27.00	0.0149
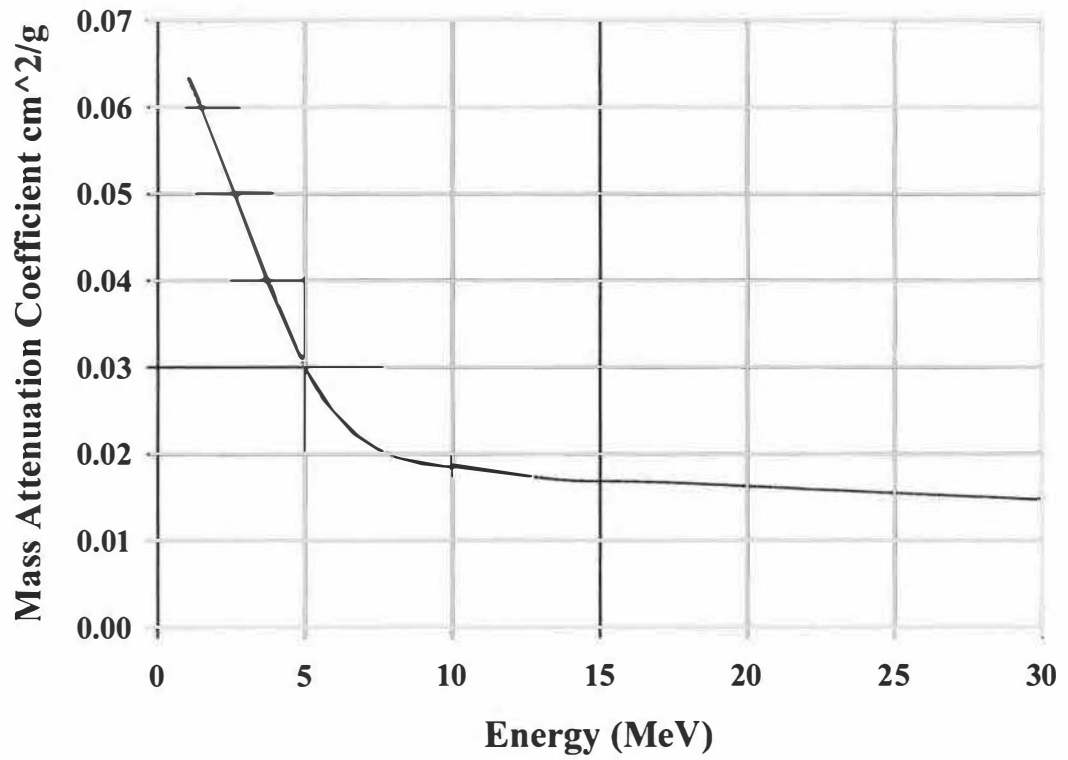
Figure 9. Mass Attenuation Coefficient for Carbon versus Energy. (Khan, F. M. 1994. "The Physics of Radiation Therapy")

Chapter 4

Setup and Data Acquisition

4.1 Setup

A Varian 6100 single 6 MV photon energy Linac and a Varian 2100C dual photon energy Linac with 6 and 18 MV photon beams were used. Figures 10, 11, 12, and 13 illustrate the setup. The attenuator was comprised of a number of 3x3 cm^2 graphite slabs 0.8 cm, 2.54 cm, 5.08 cm, 10.16cm, 20.32cm, and 40.64 cm in length, placed along the beam centerline at 100-cm SSD. Different combinations of the slabs were used to achieve a wider range of attenuating lengths. Buildup caps were placed on the ionization chambers. The purpose of the buildup cap is to achieve electronic equilibrium in open-air measurements so as to satisfy the Bragg-Gray principle. For the Varian 6100, the ionization chamber with a 6 MV build up cap was placed at distances of 123.5 cm and 184.5 cm from the 100 cm SSD. This was done to observe the effect of scatter due to distance between the attenuator material and the detector. The consistency of the measurements in producing comparable transmission ratios for different slab thickness was observed at both distances. The chamber was placed at 184.5 cm for both the 2100-6 MV and the 2100-18 MV using 6 MV and 18 MV buildup caps, respectively. Secondary blocks were positioned next to the graphite slab to further discriminate against scatter as seen in Figures 10 and 11. The chamber was also surrounded with blocks to further
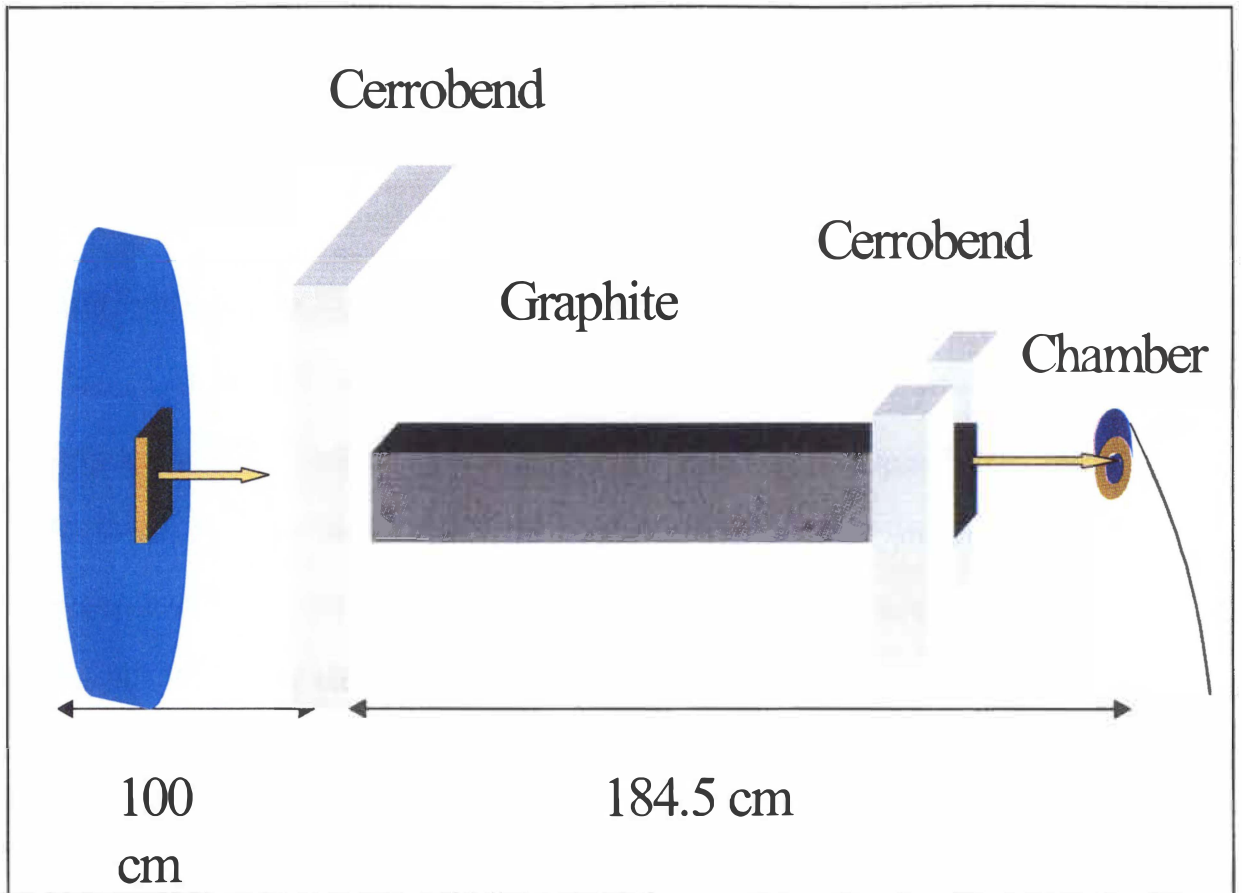
Figure 10. Experimental setup
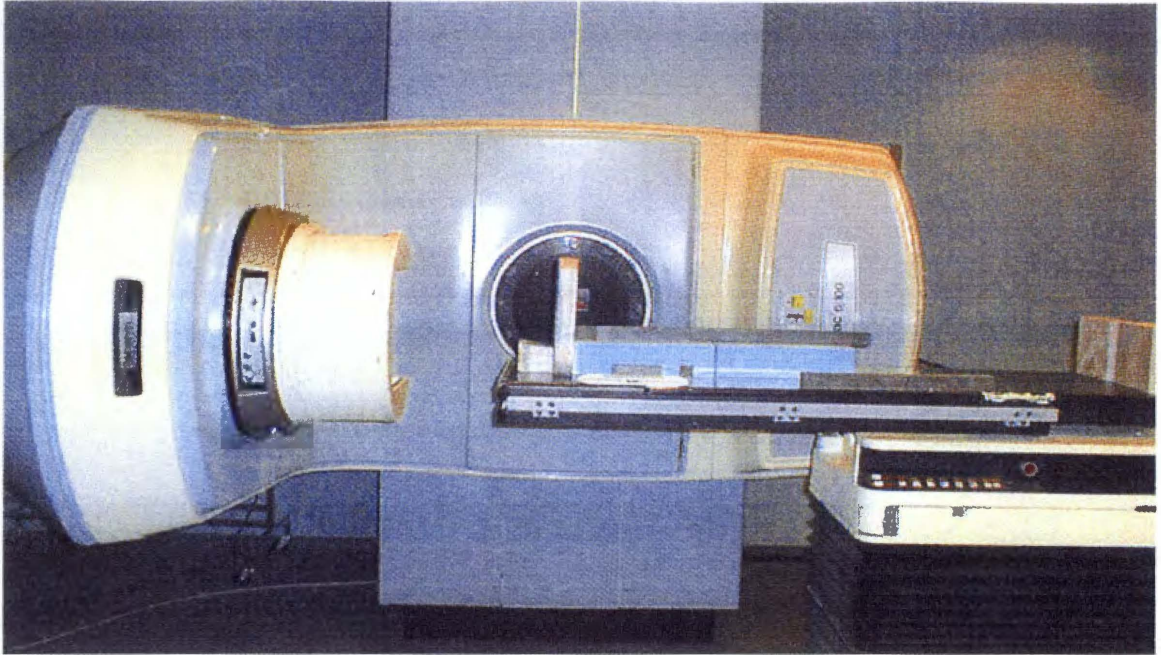
Figure 11. 6100Varian setup with the graphite attenuator placed at 100cm SSD with the NEL farmer detector on the opposite side.
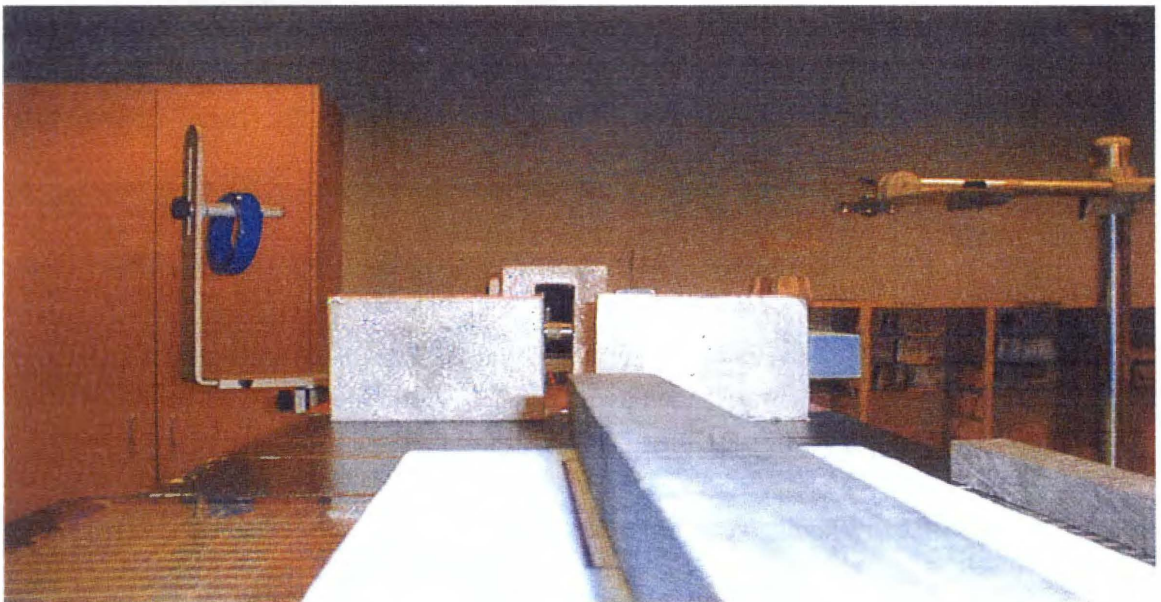
Figure 12. NEL 0.6 cm^3 farmer chamber detector placed at 184.5 cm from the SSD position. The surrounding Cerrobend blocks are used to minimize scatter contribution to detector readings.
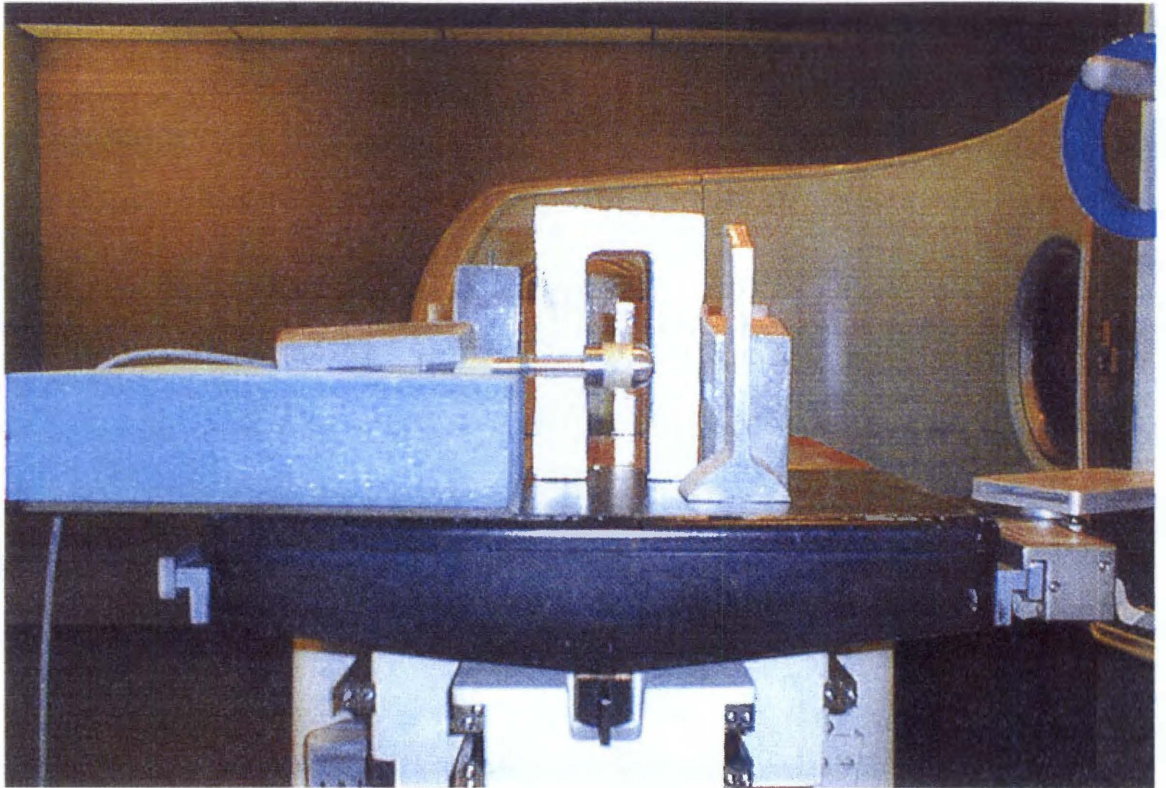
Figure 13. A view alongside the Graphite in the direction of the detector.

reduce the scatter due to scattered radiation (Figure 12). Since the slab is relatively narrow, special care was given to insure the beam is properly aligned through the central axis. A 1x1-cm^2-field size at 100 cm SSD producing 1 cGy / MU (MU = monitor unit) beam was centered at the front end of the slab.

4.2 Method of Data Collection and Analysis

Measurements were all taken along the central axis only using a Keithly 616 electrometer and NEL farmer chamber. Open-air measurements were taken as the un-attenuated signal I(0). Subsequent measurements I (x) was taken with different slab thickness where x denotes an attenuator thickness in cm. The average modal attenuation coefficient was determined by plotting transmission T(x) vs. graphite

28

thickness in cm to determine 1st, 2nd, and 3rd HVL's and by averaging the corresponding effective energies. A visual basic program was developed, using the Simpson rule technique outlined in section 3.1 to unfold the spectrum. This program uses attenuation coefficients vs. energy for graphite and combines it with the transmission versus attenuating length data to produce a meaningful energy spectrum. A model that uses 79 energies to define 79 values for the spectrum, associated with F_1 through F_{79} was chosen. The odd number of energies was picked to satisfy the requirement of the Simpson equation, the number of nodes was picked to give a resolution of more than one fractional photon fluence (F_i) per MeV. The modal energy was predetermined according to the methods described above. The initial values of F_1 through F_{79} were set to rise towards the energy associated with the modal energy and then decline towards the final energy.

Output for the program consists of:

1. The Spectrum of the beam.

2. The value of the 1st, 2nd and 3rd HVL and the corresponding effective energies along with the average modal energy.

3. The value of χ^2 and the spectrum (F_1 through F_{79}).

The unfolded spectra were compared to spectra used in the ADAC Laboratories 3DPRTP system currently used at the Thompson Cancer Survival Center (TCSC). All of the above spectra were also compared to modified Jones fit Laplace transform generated spectra

Chapter 5

Results and Discussion

5.1 Scatter Considerations

The transmission ratio data $\dfrac{I(x)}{I(0)}$ listed in Table 2 is for a chamber setup at 125.3

cm and 184.5 cm from the attenuator are almost identical for the two sets of 6 MV

measurements. Thus, we can conclude that the detector was placed at a distance

sufficiently large from the source for its response to be affected with scattered radiation.

The setup shown in Figures 10, 11 and 12 was utilized to discriminate against scatter of

the beam and leakage which is defined as all radiation originating in the gantry head of

the Linac except the useful beam (NCRP REPORT No.49, 1994, Structural Shielding

Design And Evaluation For Medical Use of X Rays And Gamma Rays Of Energies Up to

Table 2. Relative electrometer readings for a Varian 6100 6 MV and a Varian 2100 6 MV photon beam attenuated through graphite taken at distances of 125.3 cm and 184.5 cm between the source and the detector.

Graphite Slab Thickness (cm)	6100 6MV I(x)/I(0) Measurement At x=125.3cm	2100 6MV I(x)/I(0) Measurement at x = 184.5cm
2.54	0.8020	0.8027
5.08	0.6586	0.6570
17.78	0.2440	0.2429
38.10	0.0576	0.0572

10 MeV). Leakage measurements were taken behind the beam exit window and at 90 degrees off the beam's central axes at a distance of 1 m from the source. Leakage was well below 0.1% of the useful beam measured along the beam axes at 1 m SSD. Electrometer readings of the primary beam were taken with and without the Cerrobend blocks shown in Figures 11, 12, and 13. These readings were not affected by the removal of the blocks. Nevertheless, the blocks were kept to obtain maximum protection against scatter.

The open-air measurements along with the subsequent attenuation thickness electrometer readings are displayed in Table 3.and Table 4. The two tables contain the corresponding transmission data T (x) for a separation of 184.5 cm between the chamber and the source.

Table 3. Electrometer readings (nC) for the Varian 6100 6 MV beam and the 2100CD for 6 and 18MV beams.

Attenuation thickness(cm)	2100-6MV electrometer readings	6100-6MV electrometer readings	2100-18MV electrometer readings
0.00	2.271	2.036	3.220
0.80	2.043	1.818	3.017
2.54	1.823	1.651	2.780
5.08	1.492	1.417	2.553
7.62	1.206	1.142	2.246
10.16	0.999	0.978	2.010
12.70	0.813	0.816	1.796
17.78	0.552	0.562	1.443
20.32	0.463	0.489	1.298
22.86	0.381	0.412	1.165
25.40	0.320	0.352	1.048
38.10	0.130	0.156	0.677
40.64	0.113	0.137	0.623
43.18	0.094	0.119	0.562
78.74	0.009	0.015	0.147

Table 4. Transmission data $T(x) = \dfrac{I(x)}{I(0)}$ calculated using the electrometer readings in Table 3

Attenuation thickness (cm)	T(X) 2100-6 MV T(0) = 2.271 nC	T(X) 6100 T(0) = 2.036 nC	T(X)2100-18 MV T(0) = 3.220 nC
0.80	0.900	0.893	0.937
2.54	0.803	0.811	0.864
5.08	0.657	0.696	0.793
7.62	0.531	0.561	0.700
10.16	0.440	0.480	0.624
12.70	0.358	0.401	0.558
17.78	0.243	0.276	0.448
20.32	0.204	0.240	0.403
22.86	0.168	0.202	0.362
25.40	0.141	0.173	0.326
38.10	0.057	0.077	0.210
40.64	0.050	0.067	0.193
43.18	0.042	0.058	0.175
78.74	0.004	0.008	0.046

5.2 Modal Energy Results

The average modal attenuation coefficient was determined by plotting transmission T(x) vs. graphite thickness in cm, then finding the 1st, 2nd, and 3rd HVL's which correspond to effective energies as described in the Methods and Materials chapter. The average modal attenuation coefficients for the three beams and their corresponding energies are displayed in Table 5. Figure 14 is a plot of the transmission T(x) vs. Graphite thickness in cm.

Table 5. Experimentally determined average modal energies for the 6100 Varian and 2100 6 MV and 2100 18 MV photon beams.

Beam	Average Modal Attenuation Coefficient cm^2/g	Corresponding Modal Energy (MeV)
6100	0.062	0.835
2100 6 MV	0.075	0.734
2100-18 MV	0.030	4.177
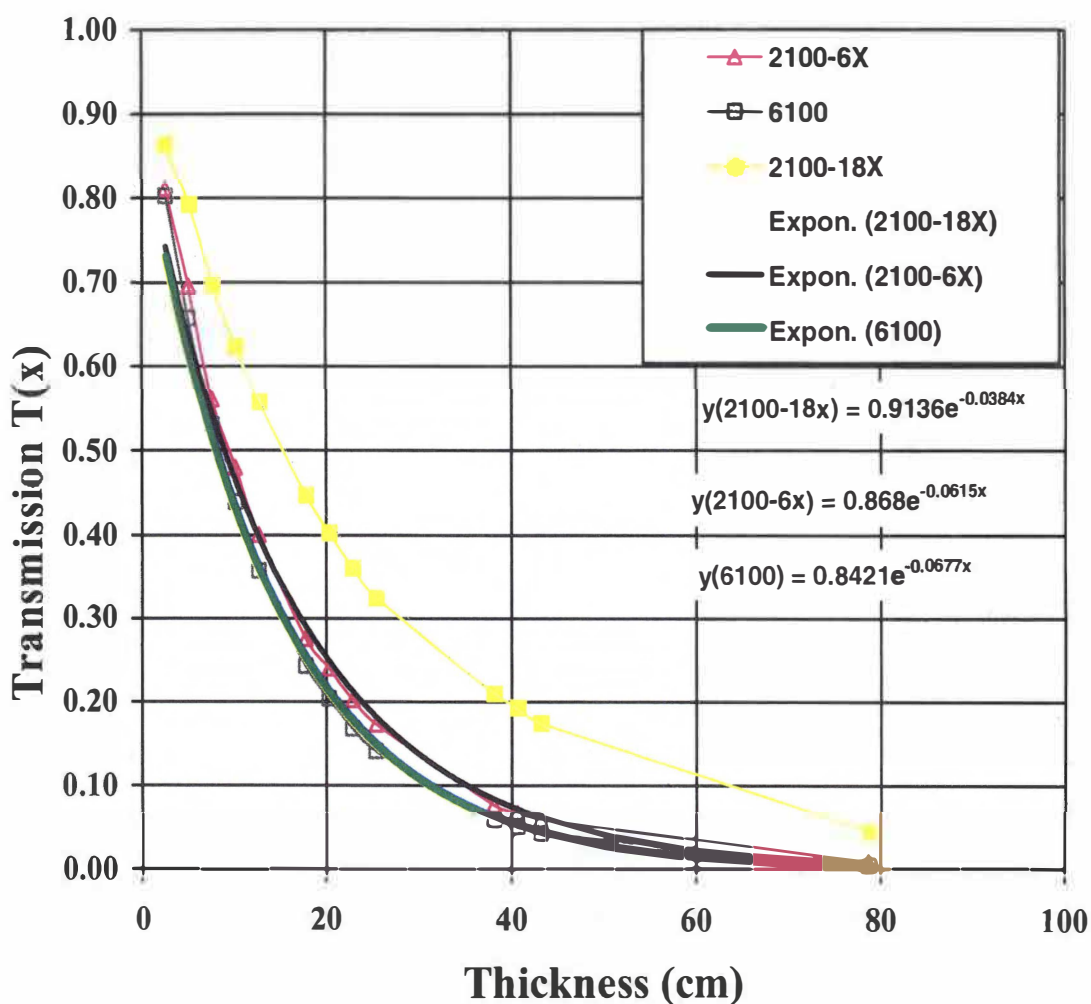
Figure 14. Transmission vs. thickness for a Graphite attenuator.
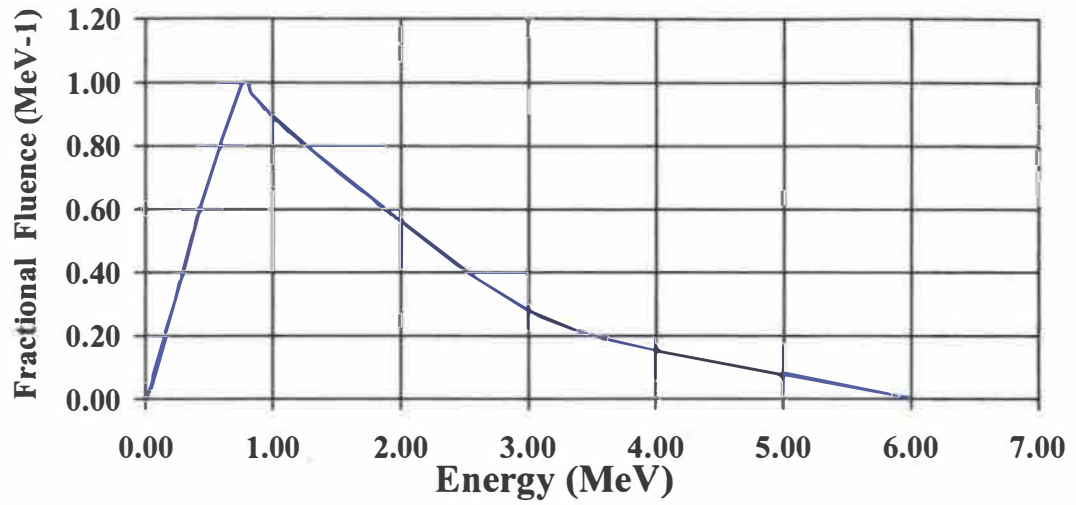
Figure 15. Simpson generated photon energy spectrum for a Varian 2100 6 MV beam. Modal Energy = 0.734 MeV.
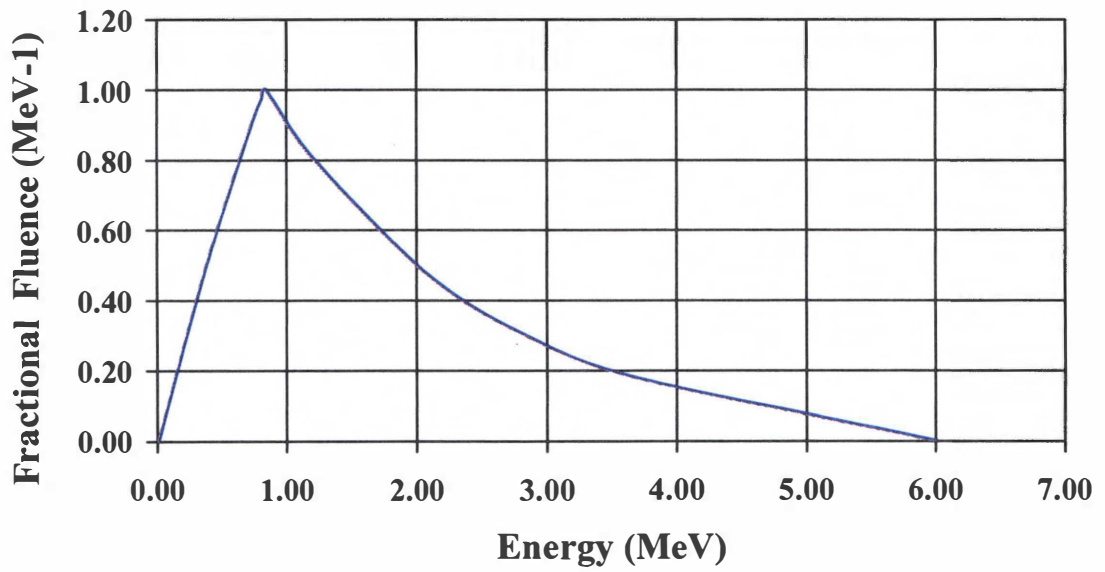
Figure 16. Simpson generated energy spectrum for a Varian 6100 6MV beam. Modal Energy = 0.835 MeV

Table 6. Ending minimized Chi square modal energy values for the Simpson generated 6 MV photon spectra.

Beam	χ^2	Modal Energy (MeV))
6100	54744	0.835
2100 6 MV	28539	0.759
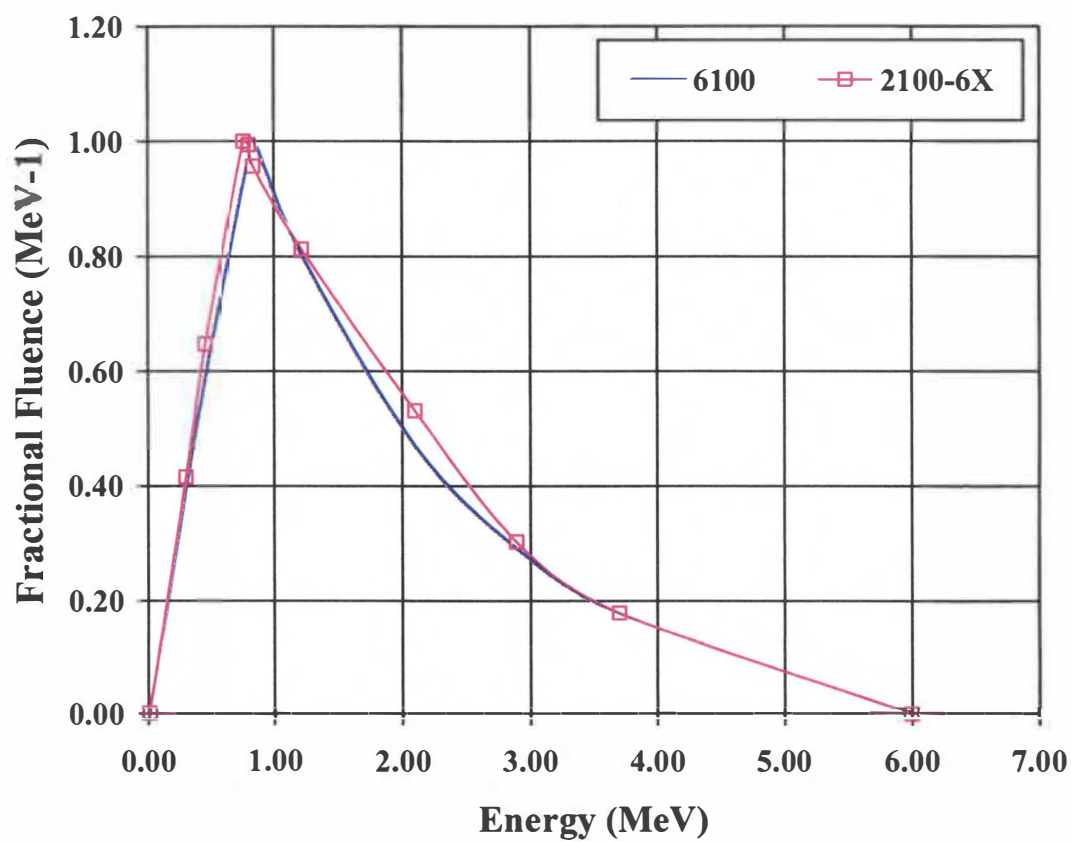
Figure 17. Simpson generated photon energy spectra of the 2100-6 MV and 6100-6 MV beams.

5.3 Resulting Spectral Model for 6 MV Beams

The resulting Simpson generated photon spectra for the 6 MV beams are shown in Figure 15, Figure 16, and Table 6.

Figure 17 is a comparative display of the two spectra. The generated spectra of this work were compared to a Mohan spectrum model used in the ADAC 3DPRTP system for the Varian 6100 and the 2100 6MV beams.

Figure 18 shows the Mohan beam spectrum model. All of the above spectra were also compared to their respective Huang modified Jones Laplace transform models. The Laplace models were generated as described in section 3.2. Figures 19 and 20 are the fitted data to equation 9. Table 7 includes the corresponding values for a and b which are used in equations 10 and 11 to generate the Laplace spectra.

Figures 21 and 22 display the Simpson generated spectra for the Varian-6100 and Varian-2100 6 MV beams vs. the Pinnacle spectrum and the Laplace spectra. Table 8 is a comparison of the modal energies for the Simpson models vs. the Pinnacle generated spectra and the modified Jones Laplace spectra. The Huang modified Jones method yielded a modal energy of 1.0 MeV for the 2100-6 MV beam and 0.7 MeV for the 6100-6 MeV beam.

5.4 Resulting Spectral Model for the 18MV Beam

The Simpson modeling technique is capable of generating energy spectral distribution for the 18 MV photon beam. The generated spectral model of this work is compared to the spectral model used in the Pinnacle 3DPRTP.
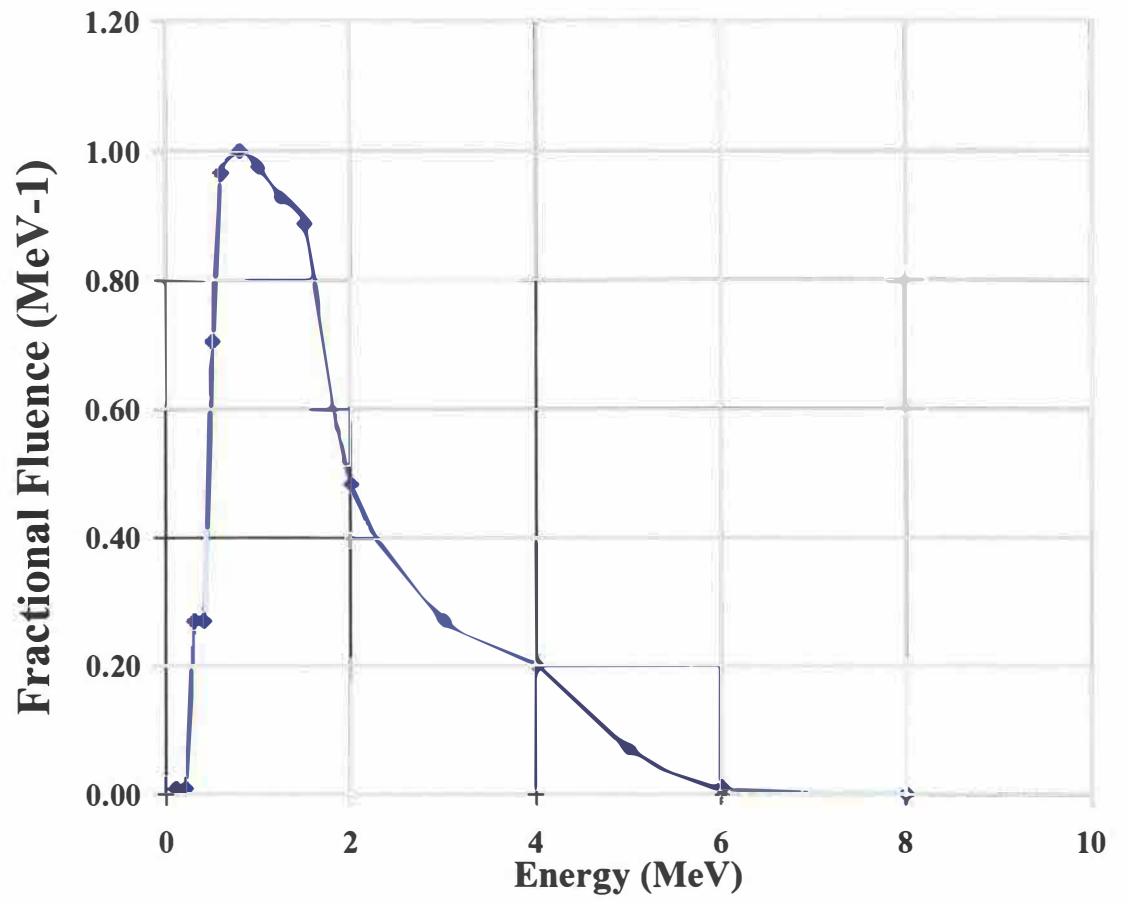
Figure 18. Pinnacle photon energy spectrum based on a Mohan Monte Carlo model.
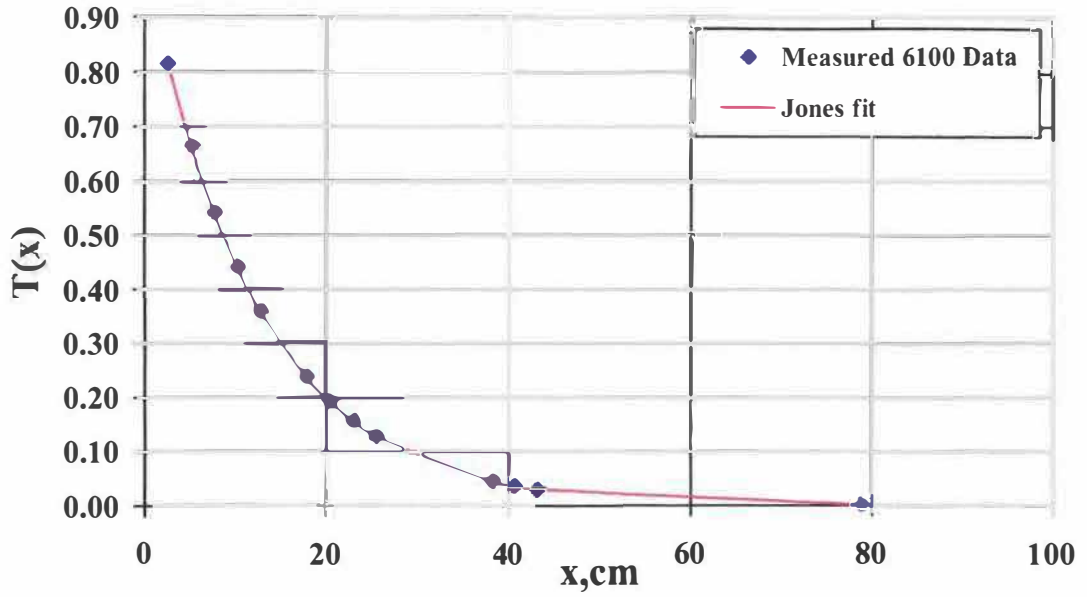
Figure 19. Huang modified Jones fit of the 6100 transmission data T(x) to the exponential function in Equation 9, $T(x) = e^{(-ax+bx^2)}$ **.**
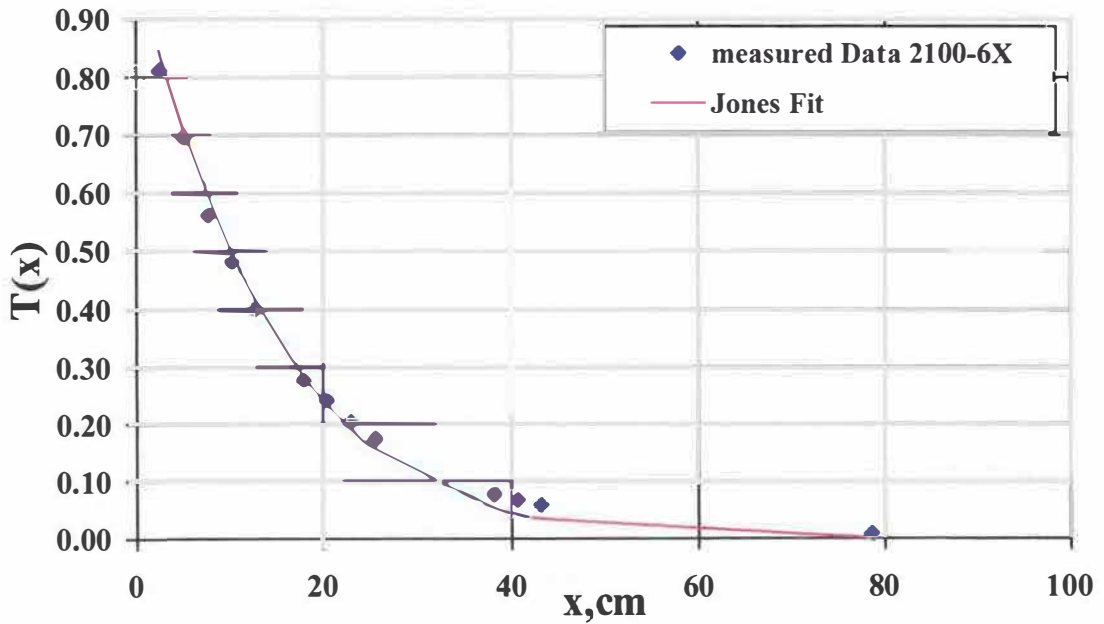
Figure 20. Huang modified Jones fit of the 2100 6 MV experimental data T(x) to the exponential function in Equation 9, $T(x) = e^{(-ax+bx^2)}$

Table 7. Fitted values of parameters a and b of equation 9, $T(x) = e^{(-ax+bx^2)}$ to the experimental attenuation data T(x) of the photon beams.

Beam	A	b
2100 6 MV	0.065	0.0003
6100	0.075	0.0004
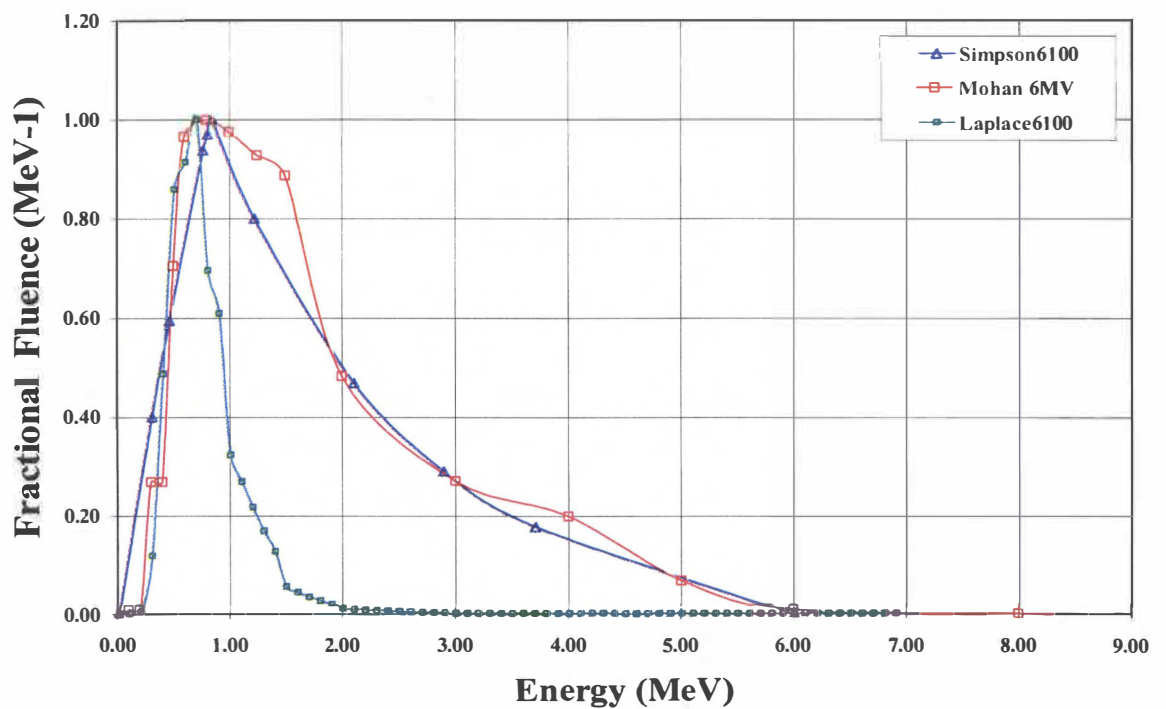
Figure 21. A comparison of the Simpson generated spectrum Versus the Pinnacle spectrum, and the modified Jones spectrum for the Varian 6100 beam.
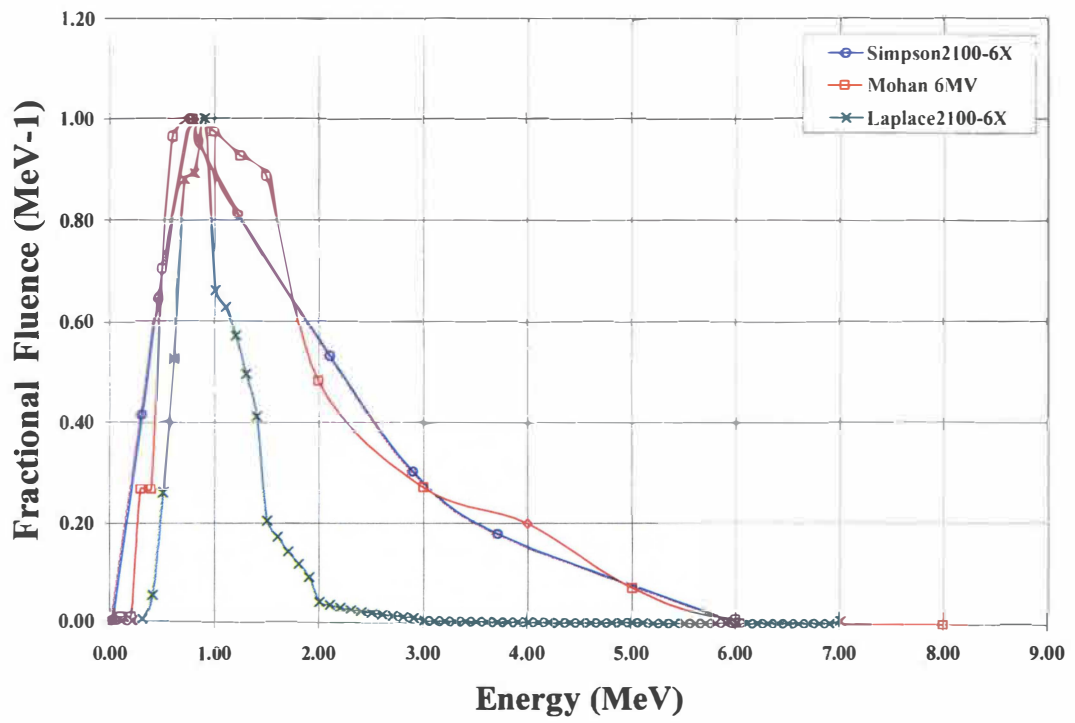
Figure 22. A comparison of the Simpson generated spectrum Versus the Pinnacle spectrum, and the Laplace modified Jones spectrum for the 2100-6X beam.

Table 8. A comparison of the modal energies for the Simpson models vs. the Pinnacle generated spectra and the modified Jones Laplace spectra.

Beam	Modal Energy MeV
Pinnacle –Mohan Monte Carlo 6MV	0.800
Simpson 2100 6 MV	0.759
Laplace 2100-6 MV	1.000
Simpson 6100	0.835
Laplace 6100	0.700

.Figures 23 and 24 displays the Simpson generated spectra for the 2100-18 MV beam vs. the Pinnacle spectrum and the Laplace spectrum Table 10 includes the corresponding values for a and b which are used in Equations 10 and 11 which were used to generate the Laplace spectra. The Laplace models were generated as described in section 3.2, figure 25 shows these data fit to Equation 9.

The Pinnacle spectral model yielded a modal Energy of 1.50 MeV, where as the Simpson model experimentally defined modal energy was 4.17 MeV, and Huang modified Jones method yielded a modal energy of 2.50 MeV. The relatively large differences in the modal energies for the 18 MV spectra lead the author to compare the results with a fourth spectral model generated by Francois and Catala through a technique of direct resolution of a matrix system of transmission data (A. Catal et al 1993). The Francois – Catala technique yields a number of modal energies for 15MV to 20 MV beam spectra ranging from 2.76 to 3.58 MeV. These modal energies agree better with the Simpson model than the interpolated 18 MV model. The collected HVL data also suggests that the modal energy of the beam is substantially larger than 1.5 MeV which is the modal energy of the interpolated ADAC 18 MV spectrum.

42
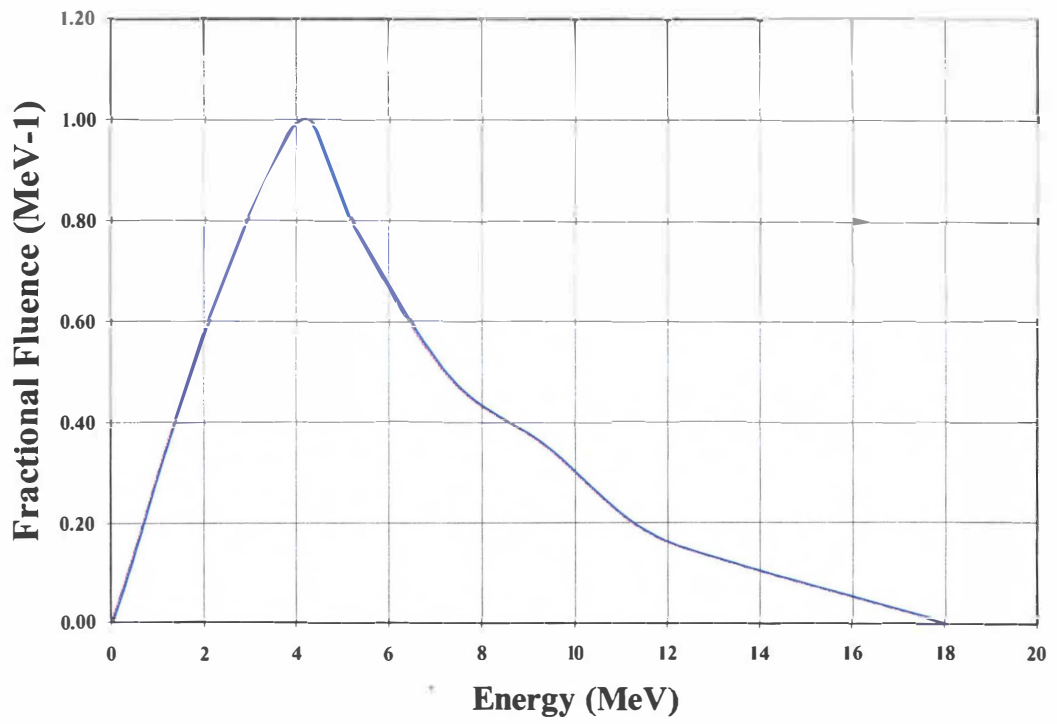
Figure 23. Energy Spectrum generated using the Simpson technique for the 2100-18 MV beam.
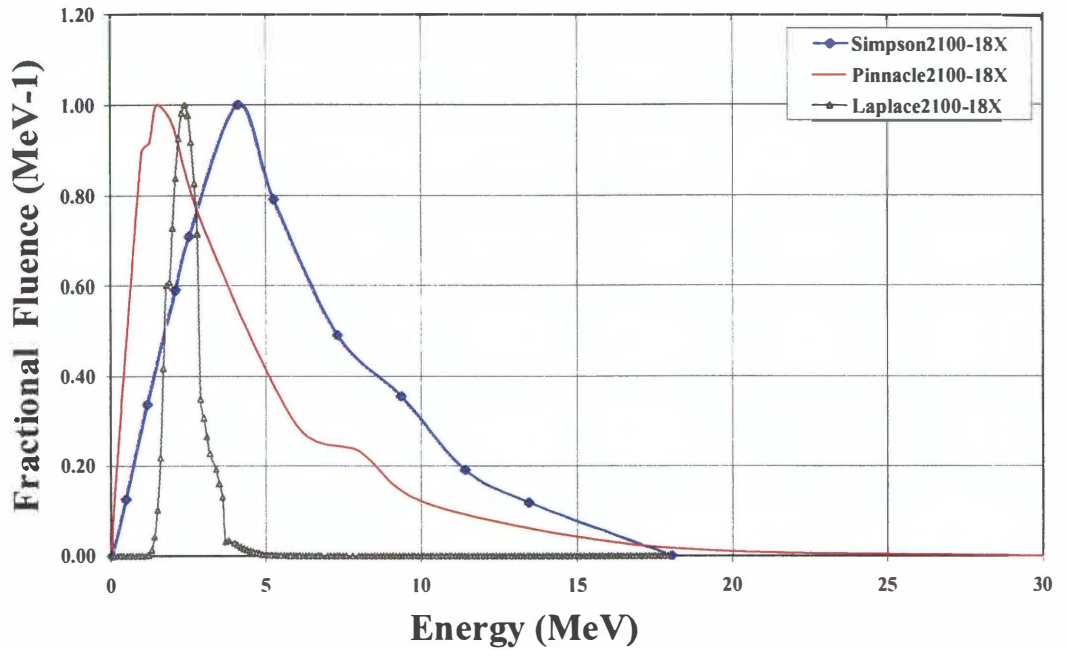
Figure 24. A comparison of the Simpson generated spectrum versus the Pinnacle spectrum and the Laplace transform for the 2100-18 MV beam.

Table 9. Modal Energy and fractional photon fluence of the modal energy for the Pinnacle, Simpson, and Laplace spectrum modeling techniques

Spectrum Type For the 2100-18 MV beam	Modal Energy MeV
Pinnacle 2100-18 MV	1.50
Laplace 2100-18 MV	2.50
Simpson 2100-18 MV	4.17

Table 10. Fitted values of parameters a and b of equation 9, $T(x) = e^{(-ax+bx^2)}$ **to the experimental attenuation data T(x) of the photon beams.**

Beam	A	b
2100-18 MV	0.04	0.000045
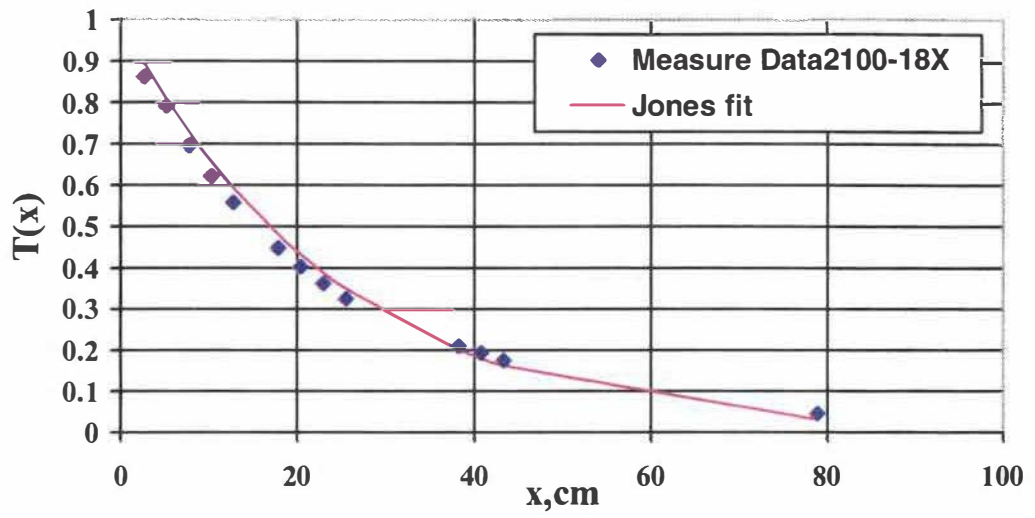
Figure 25. Huang modified Jones fit of the 2100-18 MV experimental data T(x) to the exponential function in equation 9, $T(x) = e^{(-ax+bx^2)}$.

Chapter 6

Conclusions and Future Work

6.1 Conclusion

In conclusion, the photon spectrum of a high-energy Linac can be measured through the use of a monoenergetically declining attenuation coefficient attenuator. Carbon is a good choice for such material. The attenuation data can be converted to a spectral distribution using spectral unfolding techniques. The resulting Simpson unfolded spectra's were compared to the published 6 MV Mohan spectrum and an interpolated 18MV spectrum. Both spectra's are Monte Carlo based and used in the ADAC Laboratories three dimensional Pinnacle treatment planning system. Modal energies for the Simpson technique were determined and compared to the modal energies for the Mohan spectrum and the interpolated 18 MV spectrum. Our methods modal energies for the 6MV beams were similar to the Mohan 6MV spectrum. All of the above spectra's were also compared to a Huang modified Jones-fit Laplace transform generated energy fluence spectra. The relatively large differences in the modal energies for the 18 MV spectra lead the author to compare the results with a fourth spectral model generated by Francois and Catala through a technique of direct resolution of a matrix system of transmission data. The Francois – Catala technique yields a number of modal energies which agree with the Simpson model as opposed to the interpolated 18 MV model. The HVL data also suggests that the modal energy is closer to the Simpson and Francois – Catala modal energies. The disagreement of all the above models leads the author to

conclude that further work and unification of methodology is needed to verify true photon energy spectra.

6.2 Future Work

In future work we plan to investigate resolving the photon energy spectrum via Monte Carlo calculations. We also hope to resolve the discrepancies that exist in current spectral models and thus, create a proposal for future spectral modeling criteria.

References

References

P.H Huang, K.R. Kase, and B.E. Bjarnard, "Simulation studies of 4-MV xray spectral reconstruction by numerical analysis of transmission data", Med Phys 9,695-702(1982).

A. Catala, P.Francois, and J Bonnet, "Reconstruction of 12 MV bremsstrahlung spectra from measured transmission data by direct resolution of the numeric system AF = T", Med Phys 22,3-10(1994).

P.Francois, A. Catala, Ch. Scouranec, "Simulation of xray spectral reconstruction from transmission data by direct resolution of the numeric system AF=T", Med Phys 20, 1695-1703(1993).

A. Pirametti, G. Arcovitto, and L. Azario, C.Bacci, L. Biancirdi, E De Sapio, C. Giacco, "Study of quality of bremsstrahlung spectra reconstructed from transmission measurements", Med Phys 17, 227-233(1989).

P. Bloch, J. Mcdonough, "Extraction of the photon spectra from measured beam parameters", Med Phys 25, 752-757(1998).

P.H Huang, K R. Kase, B. E. Bjarngard, "Spectral characterization of 4MV bremsstrahlung by attenuation analysis", Med Phys 8, 368-374(1981).

B. R. Archer, L.K. Wagner, "A Laplace transform pair model for spectral reconstruction", Med. Phys 9, 844-847(1982).

L. B. Levy, R. G. Wagner, A. E Wright, "Measurement of primary bremsstrahlung spectrum from an 8-MeV Linear accelerator", Med. Phys 3, 173-175(1976).

R. Mohan, C. Chui, L. Lidofsky, "Differential pencil beam dose computation model for photons", Med Phys 13, 64-73(1986).

Faiz M Khan, "The physics of Radiation Therapy", second edition 1994.

William R. Hendee and Geoffrey Ibbott, "Radiation Therapy Physics", second edition.

William R. Hendee and Russell Ritenour, "Medical Imaging Physics", third edition.

Thomas S. Curry III, James E. Dowdey, Robert C. Murry Jr., "Christensen's Physics of Diagnostic Radiology", fourth edition.

John HE Cunningham, "The physics of radiology", 3rd edition. 1969.

Appendices

Appendix A

A Visual Basic Program for the Simpson Iteration Technique
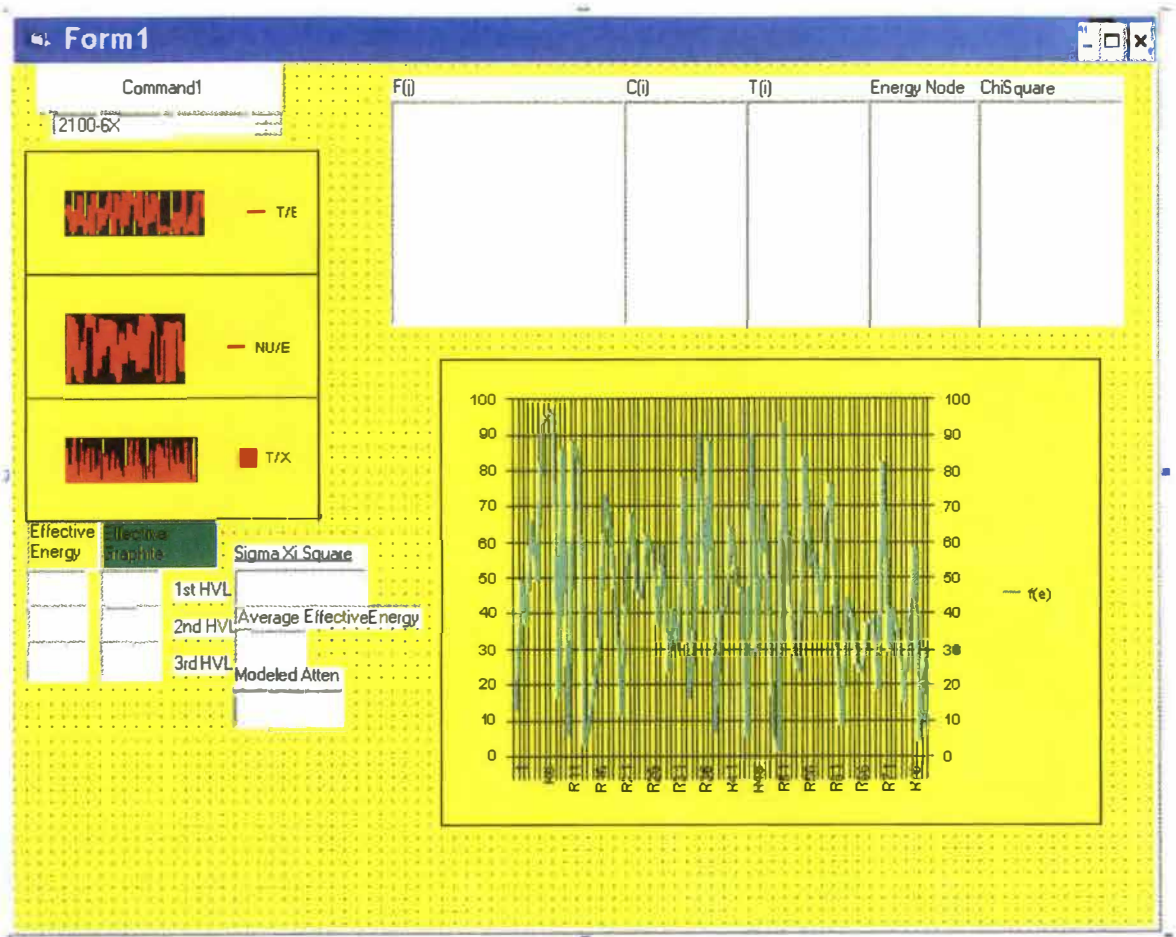
Dim f(500) As Single, T(500) As Single, Aij(200, 200) As Double, Ef As Double
Dim Ei As Double, j As Integer, nu(300) As Single, CCOUNT(5000, 5000) As Single
Dim EnergyInterval As Integer, I As Integer, e(200) As Single, Alpha As Integer
Dim c(200) As Double, X(500) As Single, Xi2 As Single, K As Integer, ci(300) As Single
Dim L As Integer, R As Integer, CHI2 As Single, m As Integer, n As Single, cprime(300), chii(300)
Dim LU As Integer, adjust As Integer, gam As Single, en As Integer, energy As Integer, evenodd As Integer, XI(300, 300) As Single, XIPRIME(300, 300) As Single
Dim TestXi(500, 500) As Double

Private Sub Command1_Click()
Sum = 0

```
List2.Clear
List3.Clear
List4.Clear
List5.Clear
List6.Clear
chi2square = 0
chi1square = 0
For I = 1 To endn
 X(I) = 0#
T(I) = 0#

Next I

test = 1E+16
' NUMBER OF SIMPSON NODES
endn = 79
' Establish initial and final energies
If List1 = "2100-18X" Then
Ef = 18#
Ei = 0.01
End If
If List1 = "2100-6X" Or List1 = "6100" Then
Ef = 6#

Ei = 0#
End If
'''''''''''''''''''''''''''''''''''''''''''''''''''''''''''''''''
' 1st energy coefficient represents LOWEST energy component
' establish energies and corresponding attenuation coefficients
' nu is energy attenuation coefficient e is the energy
For eS = 1 To endn Step 1
e(eS) = (Ef / endn) * eS
nu(eS) = 0.0603 * (e(eS) ^ -0.438)

Next eS


' divide the transmission data with a maximum of 79cm graphite into
'endn equal interval e.g 1st cut = largest X(I)
' Plot T(I) vs X(I)

If List1 = "2100-18X" Then
For I = 1 To endn
```

58

```
 X(I) = (79 / endn) * I
T(I) = 0.9115 * Exp(-(0.0384 * X(I)))
List4.AddItem T(I)
' Determine nodal energy


' Tnoatten = I(0)
Tnoatten = 1

If T(I) >= (Tnoatten / 2) - 0.015 And T(I) <= (Tnoatten / 2) + 0.015 Then
nodalt = T(I)
nodalx = X(I)
nodalnu = -Log(nodalt) / (2.265 * nodalx)
nodalE = e(nodalx)
End If
If T(I) >= (Tnoatten / 4) - 0.015 And T(I) <= (Tnoatten / 4) + 0.015 Then
second_nodalt = T(I)
second_nodalx = X(I) - nodalx
second_nodalnu = -Log(second_nodalt) / (2.265 * second_nodalx)
second_nodalE = e(second_nodalx)
End If
If T(I) >= (Tnoatten / 8) - 0.015 And T(I) <= (Tnoatten / 8) + 0.015 Then
Third_nodalt = T(I)
Third_Nodalx = X(I) - (second_nodalx) - nodalx
Third_Nodalnu = -Log(Third_nodalt) / (2.265 * Third_Nodalx)
Third_NodalE = e(Third_Nodalx)
End If
Avarage_Nodal_E = (nodalE + second_nodalE + Third_NodalE) / 3
Avarage_NodalX = (nodalx + second_nodalx + Third_Nodalx) / 3
Average_Nodalnu = (nodalnu + second_nodalnu + Third_Nodalnu) / 3
Next I
End If

If List1 = "2100-6X" Then
For I = 1 To endn
X(I) = (79 / endn) * I
T(I) = 0.9332 * Exp(-0.0713 * X(I))
List4.AddItem T(I)
' Tnoatten = I(0)
Tnoatten = 1

If T(I) >= (Tnoatten / 2) - 0.015 And T(I) <= (Tnoatten / 2) + 0.015 Then
nodalt = T(I)
nodalx = X(I)
```

```
nodalnu = -Log(nodalt) / (2.265 * nodalx)
nodalE = e(nodalx)
End If
If T(I) >= (Tnoatten / 4) - 0.015 And T(I) <= (Tnoatten / 4) + 0.015 Then
second_nodalt = T(I)
second_nodalx = X(I) - nodalx
second_nodalnu = -Log(second_nodalt) / (2.265 * second_nodalx)
second_nodalE = e(second_nodalx)
End If
If T(I) >= (Tnoatten / 8) - 0.015 And T(I) <= (Tnoatten / 8) + 0.015 Then
Third_nodalt = T(I)
Third_Nodalx = X(I) - (second_nodalx) - nodalx
Third_Nodalnu = -Log(Third_nodalt) / (2.265 * Third_Nodalx)
Third_NodalE = e(Third_Nodalx)
End If
Avarage_Nodal_E = (nodalE + second_nodalE + Third_NodalE) / 3
Avarage_NodalX = (nodalx + second_nodalx + Third_Nodalx) / 3
Average_Nodalnu = (nodalnu + second_nodalnu + Third_Nodalnu) / 3
Next I
End If

If List1 = "6100" Then
For I = 1 To endn
 X(I) = (79 / endn) * I
T(I) = 0.9274 * Exp(-0.063 * X(I))
List4.AddItem T(I)
' Tnoatten = I(0)
Tnoatten = 1

If T(I) >= (Tnoatten / 2) - 0.015 And T(I) <= (Tnoatten / 2) + 0.015 Then
nodalt = T(I)
nodalx = X(I)
nodalnu = -Log(nodalt) / (2.265 * nodalx)
nodalE = e(nodalx)
End If
If T(I) >= (Tnoatten / 4) - 0.015 And T(I) <= (Tnoatten / 4) + 0.015 Then
second_nodalt = T(I)
second_nodalx = X(I) - nodalx
second_nodalnu = -Log(second_nodalt) / (2.265 * second_nodalx)
second_nodalE = e(second_nodalx)
End If
If T(I) >= (Tnoatten / 8) - 0.015 And T(I) <= (Tnoatten / 8) + 0.015 Then
Third_nodalt = T(I)
Third_Nodalx = X(I) - (second_nodalx) - nodalx
```

60

```
Third_Nodalnu = -Log(Third_nodalt) / (2.265 * Third_Nodalx)
Third_NodalE = e(Third_Nodalx)
End If
Avarage_Nodal_E = (nodalE + second_nodalE + Third_NodalE) / 3
Avarage_NodalX = (nodalx + second_nodalx + Third_Nodalx) / 3
Average_Nodalnu = (nodalnu + second_nodalnu + Third_Nodalnu) / 3
Next I
End If



'''''''''''''''''''''''''''''''''''''''''''''''''''''''''''''''''''''''



chisquare = 30000000000#
K = Avarage_NodalX
TestXi(10, 0.1) = 0#

'Do While chisquare >= 300000
For mm = K - 1 To K + 1 Step 0.1

For nn = 0.4 To 0.008 Step -0.01

chi2square = 0#
For m = 1 To endn Step 1

If List1 = "2100-18X" Then
n = mm
f(n) = nn
'ri = 0.18
End If
If List1 = "2100-6X" Then
n = mm
f(n) = nn
'ri = 0.33
End If
If List1 = "6100" Then
n = mm
f(n) = nn
'ri = 0.32
End If
If m = n Then

f(m) = f(n)
```

```
End If
If m < n Then
sintheta = f(n) / n
f(m) = (m) * sintheta
End If
If m > n Then
sintheta = f(n) / (endn - n)
f(m) = (endn - m) * sintheta
End If
If m = 1 Or m = endn Then
f(m) = 0.001
End If

Next m


'GoTo 800


Sum = 0
chisquare = 0#




test = 1000000000
For I = 1 To endn Step 1


' Begin iteration by establishing curve fits for T(I)


""""""""""""""Standard Deviation""""""
80 If T(I) < 0.05 Then
gam = Val(0.005) 'Estimated uncertainty = 1 STD of T
Else
gam = 0.0015
```

End If

'f(j): Fraction of photons of a certain energy represented in beam
'Establish Simpson equation
Sum = 0#

evenodd = 1
 For j = 1 To endn Step 1
   DELTAE = (Ef - Ei) / (endn - 1)

        If j = 1 Then
        Alpha = 1
        End If
        If (j = 2 * (evenodd)) Then
        Alpha = 4
        Else
        If (j = 2 * (evenodd) + 1) Then
        evenodd = evenodd + 1
        Alpha = 2
        End If
        End If
        If j = endn Then
        Alpha = 1
        End If

Aij(I, j) = Alpha * Exp(-nu(j) * X(I) * 2.265)
' Sums all individual Simpson values
Sum = Sum + Aij(I, j) * f(j)

Next j

'''

' calculate C(I)
' Calculate Xi^2 pertinent to this value of I and sum to get Xi^2 for all I

' TRIANGULAR ITERATION
'''
' PREPARE CHISQUARE FOR F1 THROUGH FN ITERATION
' This loop subtracts each individual simpson value and multiplies it by
 'T(i)/C(i) then returns it to the equation
ci(I) = (DELTAE / 3) * Sum

```
'For 11 = 1 To ENDN Step 1
'Sum = Sum - Aij(I, 11) * f(11)
'f(11) = f(11) * (T(I) / ci(I))
'Sum = Sum + Aij(I, 11) * f(11)
'Next 11

' calculate adjusted C(i)
' Calculate adjusted Xi^2 pertinent to this value of I and sum to get Xi^2 for all I


ci(I) = (DELTAE / 3) * Sum

chi1square = chi1square + (Abs(ci(I) - T(I)) ^ 2 / (gam * T(I)) ^ 2)



' calculate adjusted C(i)
' Calculate adjusted Xi^2 pertinent to this value of I and sum to get Xi^2 for all I


' NODE by NODE iteration F1 through FN

List6.AddItem chi1square

 For L = 1 To endn Step 1
  XI(L, I) = (Abs(ci(I) - T(I)) ^ 2 / (gam * T(I)) ^ 2)
  Sum = Sum - Aij(I, L) * f(L)
  f(L) = f(L) * (T(I) / ci(I))
  Sum = Sum + Aij(I, L) * f(L)



  cprime(I) = (DELTAE / 3) * Sum
  XIPRIME(L, I) = (Abs(cprime(I) - T(I)) ^ 2 / (gam * T(I)) ^ 2)


 If XIPRIME(L, I) < XI(L, I) Then
chi2square = Abs(chi1square - XI(L, I))
  XI(L, I) = XIPRIME(L, I)
  ci(I) = cprime(I)
chi2square = chi2square + XI(L, I)
  Else
  chi2square = Abs(chi1square - XI(L, I))
```

64

```
      Sum = Sum - Aij(I, L) * f(L)
      f(L) = f(L) * (ci(I) / T(I))
      Sum = Sum + Aij(I, L) * f(L)
      ci(I) = (DELTAE / 3) * Sum
      XI(L, I) = (Abs(ci(I) - T(I)) ^ 2 / (gam * T(I)) ^ 2)
      chi2square = chi2square + XI(L, I)
    End If



Next L
List5.AddItem e(I)



Next I

chi2square = 0

TestXi(mm, nn) = chi1square
If List1 = "2100-18X" Then
If TestXi(mm, nn) < 29700 Then
ri = nn
GoTo 800
End If
End If

If List1 = "6100" Then
If TestXi(mm, nn) < 55700 Then
ri = nn
GoTo 800
End If

End If

If List1 = "2100-6X" Then
If TestXi(mm, nn) < 30300 Then
ri = nn
GoTo 800
End If

End If
chi1square = 0#
Next nn
```

```
Next mm


800 txti2 = e(second_nodalx)
txtj2 = second_nodalx
Txti3 = e(Third_Nodalx)
Txtj3 = Third_Nodalx
Text1 = 0.0603 * (Avarage_Nodal_E ^ -0.438)

txti = nodalE
txtj = nodalx

txti4 = Avarage_Nodal_E
txtj4 = Avarage_NodalX
For ll = 1 To endn
List3.AddItem ci(ll)
Next ll




'MSChart1.chartType = VtChChartType2dArea
FNORM = 0#
For s1 = 2 To endn
If f(s1) >= f(s1 - 1) Then
Max = f(s1)
End If
Next s1

For ll = 1 To endn
List2.AddItem (f(ll) / Max) * ri
Next ll

txtfinal = chi1square

For s = 1 To endn Step 1
MSChart1.Row = s
```

66

```
MSChart1.RowLabel = e(s)
MSChart1.Column = 1
MSChart1.Data = (f(s) / Max) * ri
Next s
For L = 1 To endn Step 1
MSChart2.Row = L
MSChart2.RowLabel = e(L)
MSChart2.Column = 1
MSChart2.Data = T(L)
Next L
For L = 1 To endn Step 1
MSChart3.Row = L
MSChart3.RowLabel = e(L)
MSChart3.Column = 1
MSChart3.Data = nu(L)
Next L
For l1 = 1 To endn Step 1
MSChart4.Row = l1
MSChart4.RowLabel = X(l1)
MSChart4.Column = 1
MSChart4.Data = T(l1)
Next l1
'Dim Msg ' Declare variable.
   ' On Error GoTo ErrorHandler  ' Set up error handler.
    PrintForm   ' Print form.
   ' Exit Sub
'ErrorHandler:
   ' Msg = "The form can't be printed."
    'MsgBox Msg  ' Display message.
   ' Resume Next


End Sub
```

Appendix B

Pinnacle 3-DPRTP Printouts

Patient Name: **tmp**		Date/Time: Mon Apr 1 14:07:42 2002	
Patient ID:		Comment:	
Plan Name:		Institution:	
Trial Name:		Physician/Physicist: /	
Revision:	**R03.P03.D04**	Planner:	

Machine: *2100C*
Version: 2001-08-14 10:48:53
Energy: *6 MV*
Field Size: All Field Sizes

Incident Fluence

Incident fluence increase/cm	0.00843402
Incident fluence cone radius (cm)	4.8004
X (perpendicular to gantry axis) (cm)	0.0259373
Y (parallel to gantry axis) (cm)	0.0360937
Gaussian height (cm)	0.077669
Gaussian width (cm)	0.953635
Jaw transmission	0.00593261

Modifiers

Modifier scatter factor	0.249999

Electron Contamination

On/Off	On
Max Depth [MAXD] (cm)	3
EC Surface Dose [ECD, 10x10] (D/Flu)	0.461904
Depth Coefficient [K] (1/cm)	3.70675
Off-axis Coefficient [OAC] (1/rad^2)	0
DF	0.101538
SF	0.656311
C1 (D/Flu)	0.00770778
C2 (D/Flu)	1.3205
C3 (1/cm)	0.980583

Spectral Factors

Off-axis softening factor	12

Modeling Geometry

Fluence grid resolution (cm)	0.40
Phantom Size - Lateral (cm)	50.00
Phantom Size - Depth (cm)	50.00

Energy Spectrum

(Energy in MeV)

Energy MeV	Rel Photons
0.10	0.004
0.20	0.004
0.30	0.120
0.40	0.120
0.50	0.314
0.60	0.430
0.80	0.445
1.00	0.434
1.25	0.413
1.50	0.395
2.00	0.215
3.00	0.121
4.00	0.089
5.00	0.032
6.00	0.004
8.00	0.000

Plan Authorization: _____ **NOT FOR CLINICAL USE** _____

Patient Name: **tmp**	Date/Time: Mon Apr 1 14:07:58 2002
Patient ID:	Comment:
Plan Name:	Institution:
Trial Name:	Physician/Physicist: /
Revision: **R03.P03.D04**	Planner:

Machine: *2100C*
Version: 2001-08-14 10:48:53
Energy: *18MV*
Field Size: All Field Sizes

Incident Fluence

Incident fluence increase/cm	0.00816823
Incident fluence cone radius (cm)	24.1393
X (perpendicular to gantry axis) (cm)	0.0256252
Y (parallel to gantry axis) (cm)	0.0365621
Gaussian height (cm)	0.0652337
Gaussian width (cm)	0.719951
Jaw transmission	0.00505577

Modifiers

Modifier scatter factor	0.5

Electron Contamination

On/Off	On
Max Depth [MAXD] (cm)	6
EC Surface Dose [ECD 10x10] (D/Flu)	0.267532
Depth Coefficient [K] (1/cm)	0.684703
Off-axis Coefficient [OAC] (1/rad^2)	0
DF	0.0152119
SF	0.99788
C1 (D/Flu)	0.000233378
C2 (D/Flu)	0.606021
C3 (1/cm)	0.0682791

Spectral Factors

Off-axis softening factor	12

Modeling Geometry

Fluence grid resolution (cm)	0.40
Phantom Size - Lateral (cm)	50.00
Phantom Size - Depth (cm)	50.00

Energy Spectrum

(Energy in MeV)

Energy MeV	Rel Photons
0.10	0.023
0.20	0.023
0.30	0.031
0.40	0.031
0.50	0.069
0.60	0.090
0.80	0.148
1.00	0.169
1.25	0.173
1.50	0.189
2.00	0.181
3.00	0.138
4.00	0.104
5.00	0.079
6.00	0.055
8.00	0.044
10.00	0.023
15.00	0.008
20.00	0.002
30.00	0.000

Plan Authorization: _____ **NOT FOR CLINICAL USE** _____

Pinnacle³
Printed 04/01/02

Machine: 2100C   Version: (uncommissioned)
Energy: 18MV
Geometry: SSD = 100 cm Field: 10 X 10

Depth Dose

Dose

Measured
Prev Comp

Distance

Pinnacle³

RTP System 6.0i   ADAC Laboratories   Milpitas, CA 95035   (800) 232 - 2123
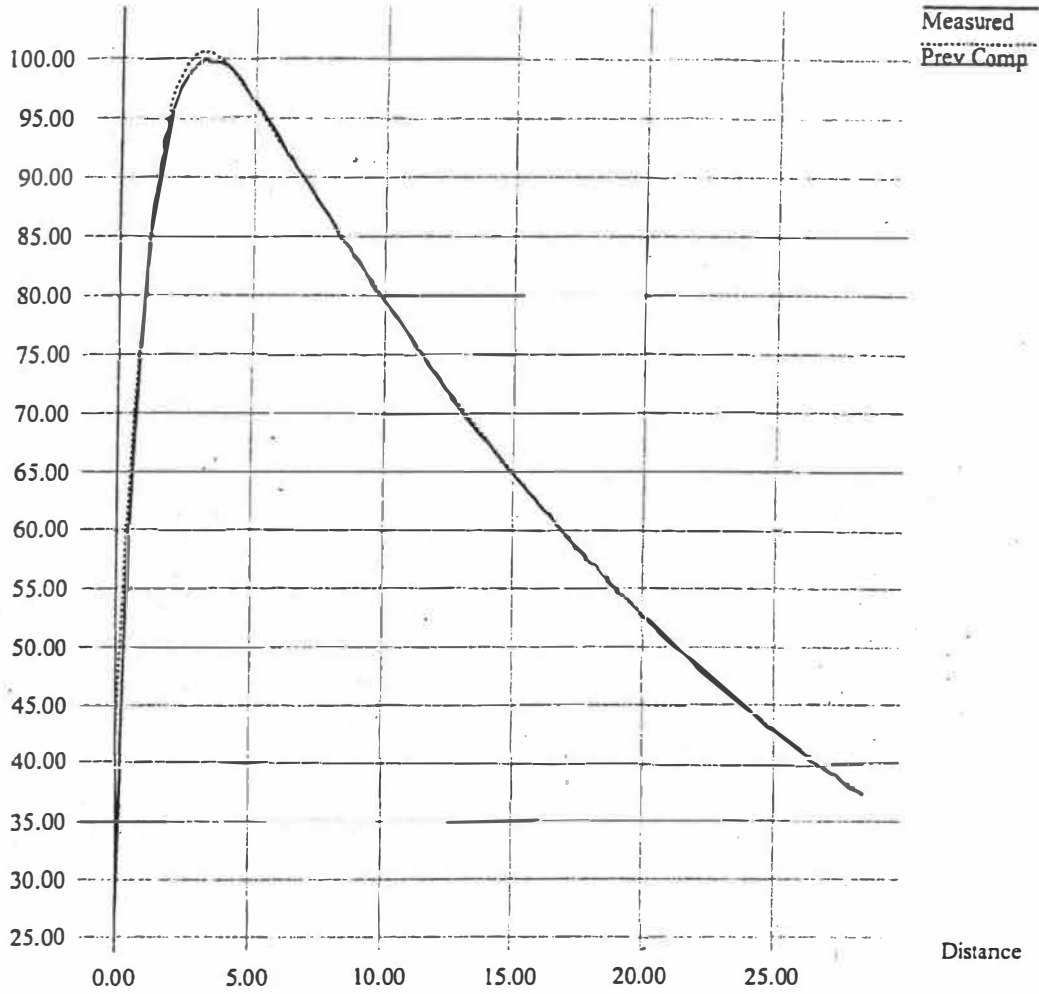
Patient Name: tmp	Date/Time: Mon Apr 1 14:07:01 2002	Revision: R03.P03.D04	Page: 1 of
Patient ID:	Comment:	Planner:	Scaling: Fill
Plan Name:	Physician/Physicist: /	Institution:	NOT FOR CLINI

Photon Electron Contamination Equations

Electron Contamination Dose Modeling

$$E.C.\,Dose(fs, r, d) = F_{Depth}(d, fs) \cdot F_{OA}(r)$$

fs = Field Size

r = Off Axis Distance

d = Depth

Depth Effect

$$F_{Depth}(d, fs) = \frac{F_{FS}(fs)}{SF} \cdot \frac{e^{-K \cdot d} - e^{-K \cdot MAXD}}{1 - e^{-K \cdot MAXD}}$$

Off Axis Effect

$$F_{OA}(r) = e^{-OAC \cdot r^2}$$

Field Size Effect

$$F_{FS}(fs) = ECD_{10 \times 10} + C_1 \cdot (fs - 10) + C_2 \cdot \left(e^{-C_3 \cdot 10} - e^{-C_3 \cdot fs} \right)$$

74
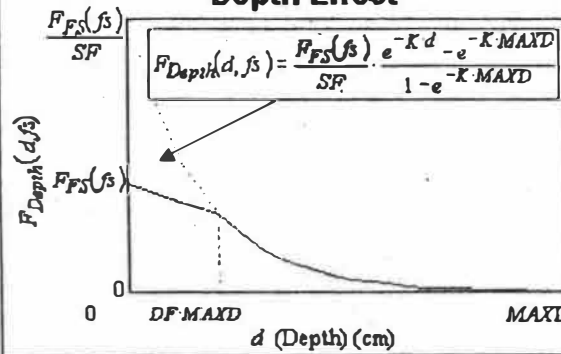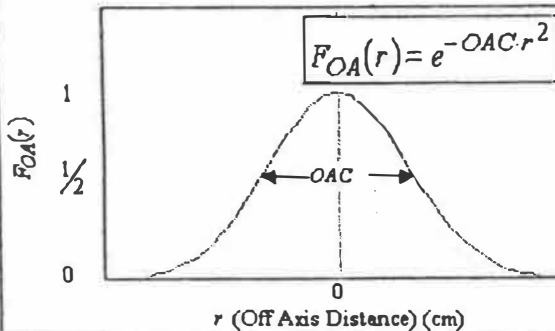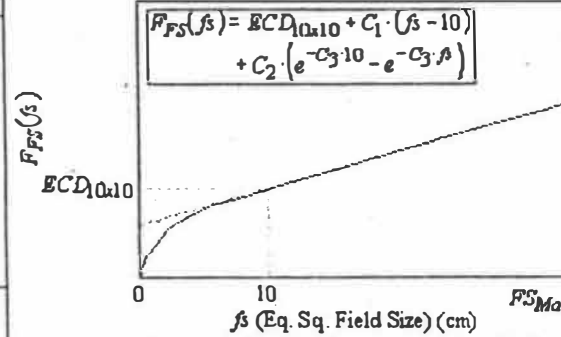
Appendix C

Huang modified Jones Laplace Transform Data and Printouts

Energy MV	F(E)	Fnew(E)
0.0	0	0
0.1	3.53139E-07	9.02465E-07
0.2	0.004099139	0.017677536
0.3	0.119537716	0.770850695
0.4	0.487893168	4.055979349
0.5	0.859727412	9.126337143
0.6	0.914284831	12.87462313
0.7	1.000804449	14.09296061
0.8	0.696045335	13.34086892
0.9	0.609449929	11.68112364
1.0	0.323441599	9.456555218
1.1	0.269878951	7.890528648
1.2	0.217724915	6.365686075
1.3	0.169829537	4.965355097
1.4	0.128080879	3.744737552
1.5	0.058569439	2.730602211
1.6	0.047226675	2.201784163
1.7	0.037579279	1.752006907
1.8	0.029907755	1.375756738
1.9	0.02247812	1.062322113
2.0	0.010279163	0.815243999
2.1	0.008725413	0.692015519
2.2	0.007372682	0.584729919
2.3	0.006201207	0.491819855
2.4	0.005192042	0.411782663
2.5	0.004327245	0.343195289
2.6	0.003590013	0.284725154
2.7	0.002964775	0.235137348
2.8	0.002437243	0.193298575
2.9	0.001994422	0.158178316
3.0	0.000952352	0.128847651
3.1	0.000842673	0.11400875
3.2	0.000744453	0.100720172
3.3	0.000656648	0.088840567
3.4	0.000578288	0.078238908
3.5	0.000508478	0.068794042
3.6	0.000446392	0.060394233
3.7	0.000391271	0.05293668
3.8	0.000342417	0.046327037
3.9	0.000299192	0.040478922
4.0	0.000174008	0.035313434
4.1	0.000158732	0.032213231
4.2	0.000144695	0.029364654
4.3	0.000131808	0.026749258
4.4	0.000119984	0.02434977
4.5	0.000109145	0.022150027
4.6	9.92155E-05	0.02013492
4.7	9.01263E-05	0.018290342
4.8	8.18125E-05	0.016603131
4.9	7.42137E-05	0.015061022
5.0	4.74873E-05	0.013652593
5.1	4.4289E-05	0.012733094
5.2	4.12918E-05	0.011871385
5.3	3.8484E-05	0.011064136
5.4	3.58546E-05	0.010308187
5.5	3.33932E-05	0.009600541
5.6	3.10899E-05	0.008938359
5.7	2.89355E-05	0.00831895
5.8	2.69209E-05	0.007739768
5.9	2.50379E-05	0.0071984
6.0	1.5034E-05	0.006692567
6.1	1.43403E-05	0.006383752
6.2	1.36766E-05	0.006088301
6.3	1.30417E-05	0.005805681
6.4	1.24345E-05	0.005535375
6.5	1.18539E-05	0.005276888
6.6	1.12987E-05	0.005029739
6.7	1.07679E-05	0.00479347
6.8	1.02606E-05	0.004567635
6.9	9.7758E-06	0.004351808
7.0	0.001390871	0.004145576

Carbon μ/ρ
2 16
0.149
0.122
0.108
0.0953
0.087
0.0805
0.0756
0.0707
0.0671
0.0635
0.06114
0.05878
0.05642
0.05406
0.0517
0.05022
0.04874
0.04726
0.04576
0.0443
0.04343
0.04256
0.04169
0.04082
0.03995
0.03908
0.03821
0.03734
0.03647
0.0356
0.03509
0.03458
0.03407
0.03356
0.03305
0.03254
0.03203
0.03152
0.03101
0.0305
0.03016
0.02982
0.02948
0.02914
0.0288
0.02846
0.02812
0.02778
0.02744
0.0271
0.02686
0.02662
0.02638
0.02614
0.0259
0.02566
0.02542
0.02518
0.02494
0.0247
0.024545
0.02439
0.024235
0.02408
0.023925
0.02377
0.023615
0.02346
0.023305
0.02315

cm^2g^-1

a	b
0.08	0.00006

$T(x) = \exp(-ax + bx^2)$

$f(new) = (1/2\sqrt{pie \cdot b})\exp(-(new-a)^2/4b)$

$f(E) = f(new) \cdot DeltaE$
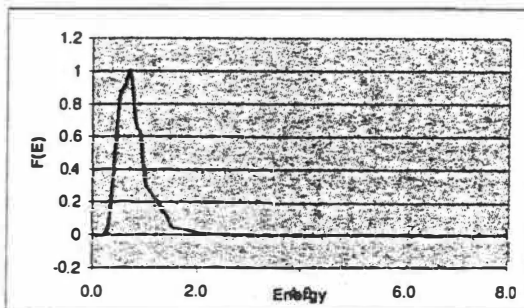
	a	b
6100	0.075	0.0004
2.54	0.824415	
5.08	0.676162	
7.62	0.551714	
10.16	0.447853	
12.7	0.361673	
17.78	0.232248	
20.32	0.184674	
22.86	0.14609	
25.4	0.114972	
38.1	0.032124	
40.64	0.024511	
43.18	0.018605	
78.74	0.000228	
81.28	0.00016	
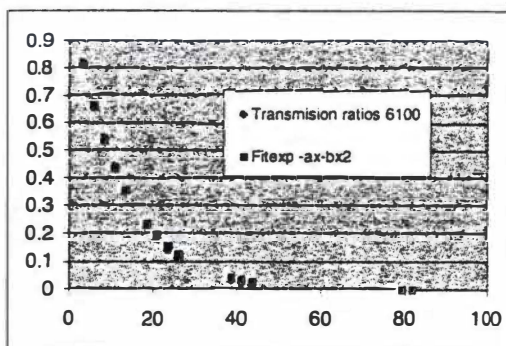
Energy MV	F(E)	Fnew(E)
0.01	0	0
0.10	3.33589E-12	7.11658E-12
0.20	9.21546E-06	3.31756E-05
0.30	0.003438546	0.018510301
0.40	0.05786604	0.401576375
0.50	0.260996505	2.312830566
0.60	0.52587579	6.181723572
0.70	0.880850611	10.35448882
0.80	0.893127205	14.29003528
0.90	1.000229765	16.00367624
1.00	0.661443648	16.14370937
1.10	0.628543186	15.34071504
1.20	0.571038469	13.93721008
1.30	0.496002175	12.10581579
1.40	0.411898079	10.05310566
1.50	0.205084877	7.981681694
1.60	0.173435374	6.749917265
1.70	0.14410136	5.608269142
1.80	0.119221443	4.578103401
1.90	0.09277943	3.660339153
2.00	0.043699345	2.89319799
2.10	0.037675412	2.494372092
2.20	0.032284156	2.13743378
2.30	0.027495981	1.820423545
2.40	0.02327541	1.540992641
2.50	0.019582755	1.296513464
2.60	0.016375652	1.084181128
2.70	0.013610428	0.901104173
2.80	0.011243286	0.744383099
2.90	0.009231305	0.611176086
3.00	0.004416032	0.498751881
3.10	0.003908841	0.441469118
3.20	0.00345265	0.389946387
3.30	0.003043308	0.343714823
3.40	0.002676875	0.302329421
3.50	0.002349628	0.265369711
3.60	0.002058064	0.232440115
3.70	0.001798901	0.203170009
3.80	0.001569078	0.177213542
3.90	0.001365748	0.15424923
4.00	0.00079085	0.133979358
4.10	0.000719114	0.121826449
4.20	0.000653276	0.110672648
4.30	0.000592912	0.10044632
4.40	0.000537625	0.0910795
4.50	0.000487038	0.082509992
4.60	0.0004408	0.074676737
4.70	0.00039858	0.067524151
4.80	0.000360068	0.060999735
4.90	0.000324974	0.055054369
5.00	0.000206842	0.049642157
5.10	0.000192164	0.0461194
5.20	0.000178445	0.042826725
5.30	0.000165628	0.039750655
5.40	0.00015366	0.036878388
5.50	0.000142491	0.034197769
5.60	0.000132072	0.031697268
5.70	0.000122358	0.029365953
5.80	0.000113306	0.027193466
5.90	0.000104875	0.025170002
6.00	6.26627E-05	0.023286281
6.10	5.95777E-05	0.022139848
6.20	5.66336E-05	0.021045777
6.30	5.38245E-05	0.020001895
6.40	5.11449E-05	0.019006105
6.50	4.85892E-05	0.018056391
6.60	4.61524E-05	0.01715081
6.70	4.38292E-05	0.016287488
6.80	4.16149E-05	0.015464627
6.90	3.95048E-05	0.014680492
7.00	0.005599975	0.013933416

Carbon $\frac{\mu}{\rho}$
2.1600
0.1490
0.1220
0.1060
0.0953
0.0870
0.0805
0.0756
0.0707
0.0671
0.0635
0.0611
0.0588
0.0564
0.0541
0.0517
0.0502
0.0487
0.0473
0.0458
0.0443
0.0434
0.0426
0.0417
0.0408
0.0400
0.0391
0.0382
0.0373
0.0365
0.0356
0.0351
0.0346
0.0341
0.0336
0.0331
0.0325
0.0320
0.0315
0.0310
0.0305
0.0302
0.0298
0.0295
0.0291
0.0288
0.0285
0.0281
0.0278
0.0274
0.0271
0.0269
0.0266
0.0264
0.0261
0.0259
0.0257
0.0254
0.0252
0.0249
0.0247
0.0245
0.0244
0.0242
0.0241
0.0239
0.0238
0.0236
0.0235
0.0233
0.0232

$$T(x)=\exp(-ax+bx^2)$$
$$f(new)=(1/2sqrt(pie*b))\exp(-(new-a)^2/4b)$$
$$f(E)=f(new)*DeltaE$$
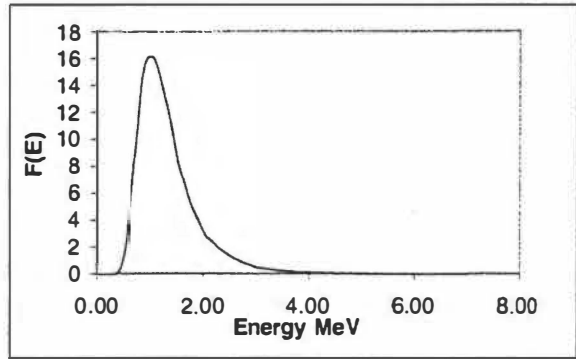
	a	b
6x	0.065	0.0003
2.54		0.84617
5.08		0.713237
7.62		0.598865
10.16		0.500891
12.7		0.417326
17.78		0.286351
20.32		0.235824
22.86		0.193462
25.4		0.158097
38.1		0.054368
40.64		0.043409
43.18		0.034526
78.74		0.000932
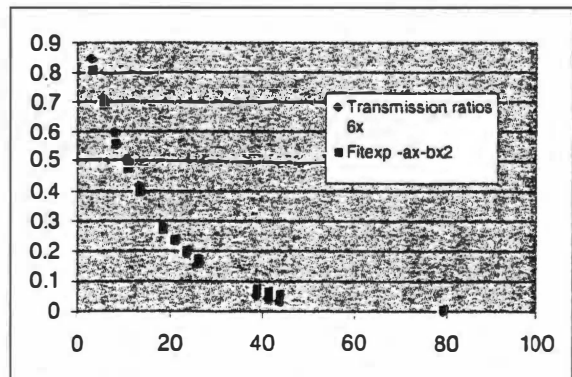
Energy MV	F(E)	Fnew(E)
0.01	0	0
0.10	5.613E-138	7.21E-03
0.20	5.544E-78	9.00E-03
0.30	1.667E-50	1.00E-02
0.40	1.854E-35	1.07E-02
0.50	1.195E-25	1.12E-02
0.60	3.948E-19	1.16E-02
0.70	8.931E-15	1.19E-02
0.80	4.081E-11	1.21E-02
0.90	1.098E-08	1.23E-02
1.00	9.648E-07	1.25E-02
1.10	1.639E-05	1.26E-02
1.20	2.065E-04	1.27E-02
1.30	1.927E-03	1.28E-02
1.40	1.333E-02	1.29E-02
1.50	4.288E-02	1.30E-02
1.60	1.026E-01	1.31E-02
1.70	2.182E-01	1.31E-02
1.80	4.180E-01	1.32E-02
1.90	6.010E-01	1.32E-02
2.00	6.083E-01	1.33E-02
2.10	7.289E-01	1.33E-02
2.20	8.385E-01	1.34E-02
2.30	9.262E-01	1.34E-02
2.40	9.822E-01	1.34E-02
2.50	1.000E+00	1.34E-02
2.60	9.776E-01	1.35E-02
2.70	9.176E-01	1.35E-02
2.80	8.269E-01	1.35E-02
2.90	7.154E-01	1.36E-02
3.00	3.484E-01	1.36E-02
3.10	3.066E-01	1.36E-02
3.20	2.661E-01	1.36E-02
3.40	2.278E-01	1.36E-02
3.50	1.922E-01	1.36E-02
3.60	1.600E-01	1.37E-02
3.70	1.313E-01	1.37E-02
3.80	3.180E-02	1.37E-02
4.00	3.452E-02	1.37E-02
4.10	2.893E-02	1.37E-02
4.20	2.409E-02	1.37E-02
4.30	1.994E-02	1.37E-02
4.40	1.640E-02	1.38E-02
4.50	1.340E-02	1.38E-02
4.60	1.089E-02	1.38E-02
4.70	8.788E-03	1.38E-02
4.80	7.050E-03	1.38E-02
4.90	5.621E-03	1.38E-02
5.00	3.144E-03	1.38E-02
5.10	2.658E-03	1.38E-02
5.20	2.240E-03	1.38E-02
5.30	1.881E-03	1.38E-02
5.40	1.576E-03	1.38E-02
5.50	1.316E-03	1.38E-02
5.60	1.095E-03	1.38E-02
5.70	9.085E-04	1.38E-02
5.80	7.515E-04	1.38E-02
5.90	6.197E-04	1.38E-02
6.00	3.290E-04	1.39E-02
6.10	2.605E-04	1.39E-02
6.20	2.319E-04	1.39E-02
6.30	2.062E-04	1.39E-02
6.40	1.831E-04	1.39E-02
6.50	1.625E-04	1.39E-02
6.60	1.440E-04	1.39E-02
6.70	1.275E-04	1.39E-02
6.80	3.383E-04	1.39E-02
7.00	8.616E-05	1.39E-02
7.10	7.482E-05	1.39E-02
7.20	6.489E-05	1.39E-02
7.30	5.621E-05	1.39E-02
7.40	4.862E-05	1.39E-02
7.50	4.201E-05	1.39E-02
7.60	3.624E-05	1.39E-02
7.80	9.369E-05	1.39E-02

Carbon $\frac{\mu}{\rho}$
2.16E+00
1.49E-01
1.22E-01
1.06E-01
9.53E-02
8.70E-02
9.05E-02
7.56E-02
7.07E-02
6.71E-02
6.35E-02
6.11E-02
5.88E-02
5.64E-02
5.41E-02
5.17E-02
5.02E-02
4.87E-02
4.73E-02
4.58E-02
4.43E-02
4.34E-02
4.26E-02
4.17E-02
4.08E-02
4.00E-02
3.91E-02
3.82E-02
3.73E-02
3.65E-02
3.56E-02
3.51E-02
3.46E-02
3.41E-02
3.36E-02
3.31E-02
3.25E-02
3.20E-02
3.05E-02
3.02E-02
2.98E-02
2.95E-02
2.91E-02
2.88E-02
2.85E-02
2.81E-02
2.78E-02
2.74E-02
2.71E-02
2.69E-02
2.66E-02
2.64E-02
2.61E-02
2.59E-02
2.57E-02
2.54E-02
2.52E-02
2.49E-02
2.47E-02
2.45E-02
2.44E-02
2.43E-02
2.41E-02
2.40E-02
2.38E-02
2.37E-02
2.36E-02
2.32E-02
2.30E-02
2.28E-02
2.27E-02
2.25E-02
2.24E-02
2.22E-02
2.21E-02

cm^2g^-1

$T(x)=\exp(-ax+bx^2)$
$f(new)=(1/2\sqrt{pie \cdot b})\exp(-(new-a)^2/4b)$
$f(E)=f(new) \cdot DeltaE$
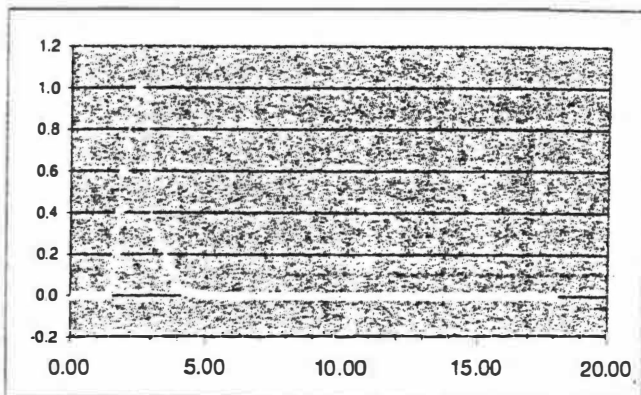
18x		a	b
		0.04	0.000045
2.54		0.903129	
5.08		0.815168	
7.62		0.735347	
10.16		0.662957	
12.7		0.597346	
17.78		0.484118	
20.32		0.435448	
22.86		0.391443	
25.4		0.35168	
38.1		0.204064	
40.64		0.182698	
43.18		0.163474	
78.74		0.032432	

- Transmission ratios 18x
- Fitexp -ax-bx2
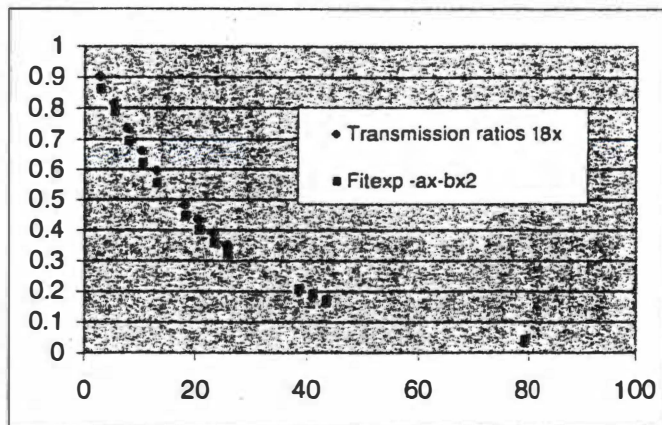
8.00	1.279E-05	1.39E-02		2.16E-02
8.10	1.158E-05	1.39E-02		2.15E-02
8.20	1.048E-05	1.39E-02		2.14E-02
8.30	9.483E-06	1.39E-02		2.13E-02
8.40	8.574E-06	1.39E-02		2.12E-02
8.50	7.747E-06	1.39E-02		2.11E-02
8.60	6.997E-06	1.39E-02		2.10E-02
8.70	6.315E-06	1.39E-02		2.09E-02
8.80	5.697E-06	1.39E-02		2.08E-02
8.90	5.137E-06	1.39E-02		2.07E-02
9.00	4.629E-06	1.39E-02		2.06E-02
9.10	4.170E-06	1.39E-02		2.05E-02
9.20	3.753E-06	1.39E-02		2.04E-02
9.30	3.377E-06	1.39E-02		2.03E-02
9.40	3.037E-06	1.39E-02		2.02E-02
9.50	2.729E-06	1.39E-02		2.01E-02
9.60	2.452E-06	1.39E-02		2.00E-02
9.70	2.201E-06	1.39E-02		1.99E-02
9.80	1.975E-06	1.39E-02		1.98E-02
9.90	1.771E-06	1.39E-02		1.97E-02
10.00	8.256E-07	1.39E-02		1.96E-02
10.10	7.797E-07	1.39E-02		1.95E-02
10.20	7.363E-07	1.39E-02		1.95E-02
10.30	6.952E-07	1.39E-02		1.94E-02
10.40	6.564E-07	1.39E-02		1.94E-02
10.50	6.196E-07	1.40E-02		1.93E-02
10.60	5.847E-07	1.40E-02		1.93E-02
10.70	5.518E-07	1.40E-02		1.92E-02
10.80	5.206E-07	1.40E-02		1.92E-02
10.90	4.911E-07	1.40E-02		1.91E-02
11.00	4.633E-07	1.40E-02		1.91E-02
11.10	4.369E-07	1.40E-02		1.90E-02
11.20	4.120E-07	1.40E-02		1.90E-02
11.30	3.884E-07	1.40E-02		1.89E-02
11.40	3.662E-07	1.40E-02		1.89E-02
11.50	3.452E-07	1.40E-02		1.88E-02
11.60	3.253E-07	1.40E-02		1.88E-02
11.70	3.065E-07	1.40E-02		1.87E-02
11.80	2.888E-07	1.40E-02		1.87E-02
11.90	2.720E-07	1.40E-02		1.86E-02
12.00	2.562E-07	1.40E-02		1.86E-02
12.10	2.413E-07	1.40E-02		1.85E-02
12.20	2.272E-07	1.40E-02		1.85E-02
12.30	2.139E-07	1.40E-02		1.84E-02
12.40	2.014E-07	1.40E-02		1.84E-02
12.50	1.895E-07	1.40E-02		1.83E-02
12.60	1.783E-07	1.40E-02		1.82E-02
12.70	1.678E-07	1.40E-02		1.82E-02
12.80	1.579E-07	1.40E-02		1.81E-02
12.90	1.485E-07	1.40E-02		1.81E-02
13.00	1.397E-07	1.40E-02		1.80E-02
13.10	1.313E-07	1.40E-02		1.80E-02
13.20	1.235E-07	1.40E-02		1.79E-02
13.30	1.161E-07	1.40E-02		1.79E-02
13.40	1.091E-07	1.40E-02		1.78E-02
13.50	1.025E-07	1.40E-02		1.78E-02
13.60	9.636E-08	1.40E-02		1.77E-02
13.70	9.054E-08	1.40E-02		1.77E-02
13.80	8.505E-08	1.40E-02		1.76E-02
13.90	7.989E-08	1.40E-02		1.76E-02
14.00	7.503E-08	1.40E-02		1.75E-02
14.10	7.045E-08	1.40E-02		1.75E-02
14.20	6.614E-08	1.40E-02		1.74E-02
14.30	6.209E-08	1.40E-02		1.74E-02
14.40	5.828E-08	1.40E-02		1.73E-02
14.50	5.469E-08	1.40E-02		1.73E-02
14.60	5.132E-08	1.40E-02		1.72E-02
14.70	4.815E-08	1.40E-02		1.72E-02
14.80	4.516E-08	1.40E-02		1.71E-02
14.90	4.236E-08	1.40E-02		1.71E-02
15.00	1.833E-08	1.40E-02		1.70E-02
15.10	1.780E-08	1.40E-02		1.70E-02
15.20	1.728E-08	1.40E-02		1.70E-02
15.30	1.677E-08	1.40E-02		1.69E-02
15.40	1.628E-08	1.40E-02		1.69E-02
15.50	1.580E-08	1.40E-02		1.69E-02
15.60	1.533E-08	1.40E-02		1.69E-02
15.70	1.488E-08	1.40E-02		1.68E-02
15.80	1.444E-08	1.40E-02		1.68E-02
15.90	1.402E-08	1.40E-02		1.68E-02
16.00	1.360E-08	1.40E-02		1.68E-02

Vita

Robbie Alhakeem was born in Essex, England on March 21, 1968. He attended schools in England, Lebanon, and France. He graduated high school in. August of 1987, he entered the University of Tennessee to pursue a degree in Nuclear Engineering. In May of 1993 he received a Bachelor of Science in that discipline. After traveling for two years, he enrolled part time in the Masters program to pursue an advanced degree in Nuclear Engineering with a concentration in Medical Physics. In 1996 he was accepted as a resident at the Thompson Cancer Survival Center in Knoxville, Tennessee where he received a formal rigorous training in clinical Medical Physics. His Masters degree was received in December of 1999.

He is presently working as a consultant at RadPhys LLC Providing a variety of services in the areas of cancer patient care, 3-D treatment planning, radiation safety, and ongoing medical physics research.